Sensors & Diagnostics

CRITICAL REVIEW

View Article Online
View Journal | View Issue

Cite this: *Sens. Diagn.*, 2023, **2**, 1077

Fluorescence probes for lung carcinoma diagnosis and clinical application

Xiaoyu Zhang,†[ab] Feifei Yu,†[ad] Zhenkai Wang,†[ad] Tongmeng Jiang,[ad] Xinyu Song*[c] and Fabiao Yu *[ad]

Lung carcinoma is the largest cause of mortality globally, making it the biggest public health issue and a significant barrier to extending human life expectancy. The specific etiology and production process of lung carcinoma are not yet known, and it has a relatively complex and multi-stage occurrence. Early detection and treatment of lung carcinoma can greatly improve the five-year survival rate. Because pre-carcinomatous tumors are small and uncharacteristic in form, early carcinomas are challenging to immediately diagnose with magnetic resonance imaging (MRI), X-ray photography, computed tomography (CT), positron emission tomography (PET), or ultrasonography (US). In order to capitalize on the particular characteristics of carcinoma, methods that can emphasize the molecular distinction between carcinoma and healthy tissue are desperately needed. With the development of bioimaging technology, fluorescent probes present a potential solution to this clinical problem. Fluorescent probes have been considered to be effective chemistry tools for achieving early detection and identification of tumor lesions, because molecular imaging technology can explicitly illustrate lesion boundary information during surgery. Fluorescent probes can also qualitatively and quantitatively analyze the lesion state at the cellular and molecular levels in the living body. This review will cover and provide an overview of the most recent developments in fluorescence probe technology for the accurate detection and clinical therapy of lung carcinoma. We anticipate that this review will serve as a spark for the development of intelligent molecular fluorescent probes for lung carcinoma clinical image-guided surgery and imaging diagnosis.

Received 1st February 2023,
Accepted 13th June 2023

DOI: 10.1039/d3sd00029j

rsc.li/sensors

1. Introduction

The near-infrared (NIR) fluorescence imaging technology is an active and non-invasive molecular imaging method.[1] The rapid development and improvement of near-infrared fluorescent probes have improved some optical properties, such as hydrophilicity, stability, and high quantum yields.[2] These features can greatly strengthen the detection selectivity and sensitivity. An excellent NIR imaging probe requires excellent chemical and photophysical properties. The spectrum of the NIR fluorescent reagent should be in the NIR range, *i.e.*, 650–950 nm (near-infrared I region), 1000–1350 nm (near-infrared II region), and 1500–1800 nm (near-infrared NIR III region)[3] to reduce the interference from the autofluorescence and increase the tissue penetration depth. Many NIR fluorophores exhibit excellent properties for selective accumulation in tissues, organs, or tumor lesions *in vivo*, and enhance tumor sites by binding to tumor-specific molecular biomarkers such as proteases, peptides, and antibodies.[2,4–7] NIR probes that possess specificity and sensitivity toward tumor sites have been widely utilized in tumor-targeted imaging and tumor treatment.[8] These probes indicate unique optical and biomedical imaging properties for broad development prospects.

Lung carcinoma displays the highest morbidity and mortality among various malignant tumors.[9] The complete resection of the lesion site, the negative margin, and clean of metastatic lymph nodes determine the prognosis of carcinoma patients.[10–12] Lung carcinoma is still a challenging problem.[13–23] It is expected that the development of fluorescent probes can serve the clinical work well, so the

[a] *Key Laboratory of Hainan Trauma and Disaster Rescue, The First Affiliated Hospital of Hainan Medical University, Hainan Medical University, Haikou 571199, China. E-mail: yufabiao@hainmc.edu.cn*
[b] *Department of Pulmonary and Critical Care Medicine, Yantai Affiliated Hospital of Binzhou Medical University, Yantai 264100, China*
[c] *State Key Laboratory of Respiratory Disease, Guangzhou Institute of Respiratory Health, National Clinical Research Center for Respiratory Disease, The First Affiliated Hospital of Guangzhou Medicine University, Guangzhou 510120, China. E-mail: songxinyu@stu.gzhmu.edu.cn*
[d] *Key Laboratory of Emergency and Trauma, Ministry of Education, Engineering Research Center for Hainan Bio-Smart Materials and Bio-Medical Devices, Key Laboratory of Hainan Functional Materials and Molecular Imaging, College of Emergency and Trauma, Hainan Medical University, Haikou 571199, China*
† These authors contributed equally to this work.

clinical application strategy of fluorescence-guided surgery (FGS) can be realized. During the surgical procedure, the fluorescent probes are used for the specific visual imaging of the lesion site to detect and discriminate malignant and normal tissues, which can reduce the surgical trauma and improve the prognosis of patients.[24,25] Compared with other traditional medical imaging models, such as magnetic resonance imaging (MRI), X-ray photography, computed tomography (CT), positron emission tomography (PET), or ultrasonography (US), FGS has its own unique safe, effective, and real-time technique for lung carcinoma surgery.[26] Near-infrared fluorescence imaging to guide surgery is conducive to the development of clinical medicine. Also, fluorescence imaging has breathed new life into surgical oncology and is expected to have a considerably essential impact on personalized oncology in the future. In this review, we will dedicatedly focus on fluorescent probes and the specific response methods for the potential application of lung carcinoma diagnosis in clinical. We also exclusively highlight near-infrared probes for fluorescence-navigation surgery and the clinical application of near-infrared tumor-targeted probes in lung surgery.

2. Probes based on the tumor microenvironment

The tumor microenvironment (TME) is the "soil" for tumor survival and is a highly complex multicellular ecosystem, including different immune cells, endothelial cells, fibroblasts, blood vessels, cytokines, and their metabolites.[27] It involves multiple factors such as molecules, cells, organs, and hosts. Interactions of the components influence disease progression and prognosis.[28] Many tumor markers are also related to microenvironment metabolism. Therefore, as a therapeutic target, the tumor microenvironment has attracted much more attention than ever before. At present, there are lots of research on the targeted regulation of cholesterol metabolites, reactive oxygen species (ROS), macrophage conversion, and vascular endothelial growth factor (VEGF), as well as carcinoma markers for carcinoma prevention or treatment.[29,30]

Hypoxia is a general phenomenon in human tumors.[31] The oxygen of most tumor lesions is lower than the normal physiological tissue level. In solid tumors, the arterial oxygen partial pressure is close to ~0 mmHg. The hypoxic

Xiaoyu Zhang

Xiaoyu Zhang received her Master's degree in Clinical Medicine from Binzhou Medical University in 2018. Currently, she is working as a doctor at the Department of Pulmonary and Critical Care Medicine, Yantai Affiliated Hospital of Binzhou Medical University. Her main research field is the imaging of small molecular fluorescence probes for lung diseases.

Feifei Yu

Feifei Yu received her Bachelor's degree in Applied Chemistry from Shandong Normal University in 2006. Then she works as a laboratory technician at Hainan Medical University now. Her main research areas are marine drug analysis and design and synthesis of fluorescent probes.

Zhenkai Wang

Zhenkai Wang received his Master's degree in Clinical Medicine from Binzhou Medical University in 2020. Now he is a PhD candidate at The First Affiliated Hospital of Hainan Medical University, Hainan Medical University. His main research direction is the design and application of small molecule fluorescent probes for clinical medical detection.

Tongmeng Jiang

Tongmeng Jiang received his Bachelor of Medicine and Ph.D. in Surgery from Guangxi Medical University in 2018. He finished his postdoc at the School of Materials Science and Engineering, Zhejiang University, in May 2022, and then he joined Hainan Medical University as an associate professor. His research focuses on biomaterials, tissue regeneration, translational medicine, imaging and oncology.

environment can prevent cell apoptosis, as well as resisting chemotherapy and radiotherapy.[32] Hypoxic tumors show stronger invasion, growth, and metastasis, resulting in poor treatment effects.[33] Therefore, it is believed that hypoxia as a characteristic tumor microenvironment can become a breakthrough for clinical therapy.[34]

Nitroreductases (NTRs) are a class of cytoplasmic enzymes that depend on the action of flavin mononucleotide or flavin adenine dinucleotide. NTRs can effectively reduce aromatic nitro compounds to their corresponding amino compounds.

Many examinations have shown that they are more abundant in hypoxic tissues, cells, and malignancies than under normal circumstances, therefore, NTRs can be utilized as a key indicator to assess the hypoxic status of cells or organisms. NTRs also play a significant role in the activation of pharmaceuticals; they have been widely employed in the treatment of tumors as promising inhibitors. Jiang *et al.* designed and synthesized a ratiometric fluorescent probe, $CyNNO_2$ (Fig. 1).[35] The probe utilized nicotinamide adenine dinucleotide phosphate oxidase (NADPH) as an electron donor to enable nitroreductases to selectively reduce nitro groups to hydroxylamine or ammonia under anoxic conditions. The *p*-nitrobenzyl moiety, as a response unit, could selectively react with NTRs. When reacted with the target detection substance, the fluorescence intensity at 805 nm gradually weakened, and the fluorescence intensity at 747 nm was detected. The detection limit of $CyNNO_2$ for nitroreductases was 0.0058 ng mL^{-1}. The probe was successfully used to detect endogenous NTRs in A549 cells (human lung carcinoma cell line) under hypoxia.

Ma *et al.* designed and synthesized an off–on fluorescent probe ($RHC\text{-}NO_2$) to detect NTRs in hypoxic tumor cells.[36] The probe fluorescence was in the second near-infrared window and had a lower detection concentration (5.9 ng mL^{-1}). When the probe was intravenously injected into A549 tumor-bearing mice, the fluorescence intensity at the tumor site reached the highest level after 12 h and could be retained for 24 h. The high sensitivity of the probe made it image tumor tissue by detecting NTRs accurately.

Li *et al.* designed and synthesized five NTR probes with distinct nitro aromatic groups (Cy7-1 to Cy7-5); however, only the *para*-nitro aromatic group chemically modified cyanine probe through the ester bond linked probe (Cy7-1) exhibited a significant response (<1 min) to NTRs.[37] The reaction mechanism was an electro-withdrawing group-induced electron-transfer process that became blocked when Cy7-1 was catalytically reduced to $Cy7\text{-}NH_2$ by NTRs, with fluorescence turn-on (*ca.* 110-fold). A549 cells cultured with different oxygen contents (20%, 10%, 5%, 3%, and 1%) showed gradually increasing fluorescence intensity after Cy7-1 incubation. Moreover, Cy7-1 not only could be used to distinguish the hypoxia degree of different tumors, but also discriminated hypoxic tumor tissues and inflammatory tissues, which further highlighted the potential diagnostic value of Cy7-1.

3. Probes based on identifying molecular markers

Heme oxygenase is composed of two structurally related isoenzymes, heme oxygenase 1 and heme oxygenase 2. Some research has shown that heme oxygenase 2 (HMOX2) is the key enzyme for removing ROS from cells.[38] ROS-mediated apoptosis induction is one of the methods for carcinoma targeted therapy. Therefore, tumor cell death can be induced by inhibiting HMOX2 activity to accumulate ROS in carcinoma cells. Vimentin, known as a marker of epithelial–mesenchymal transition (EMT), is also associated with distinguished tumor ability.[39] Human NAD(P)H quinone oxidoreductase 1 (hNQO1) is a significantly expressed enzyme in tumor tissues and one key in carcinoma therapy.[40,41] Human neutrophil elastase (HNE) plays important roles in immune response and inflammation. HNE exhibits a close relationship with lung carcinoma and acute lung injury.[42] Therefore, it is particularly important for rapid and accurate detection of NE activity.

Xinyu Song

Xinyu Song received his Doctor's degree in Internal Medicine from Guangzhou Medical University in 2021. He is now serving for Guangzhou Institute of Respiratory Health, The First Affiliated Hospital of Guangzhou Medicine University as a respiratory physician. His current interests are development of fluorescence bioimaging and theranostic tools.

Fabiao Yu

Prof. Fabiao Yu received his Ph.D. degree from Dalian University of Technology and Dalian Institute of Chemical Physics, Chinese Academy of Sciences in 2013. After four years' work at Yantai Institute of Coastal Zone Research, Chinese Academy of Sciences as an associate professor, he joined Hainan Medical University from 2018 as a full professor. His research interests focus on molecular diagnosis of tropical diseases, multi-modal visual surgery navigation, and point-of-care testing (POCT) technology.

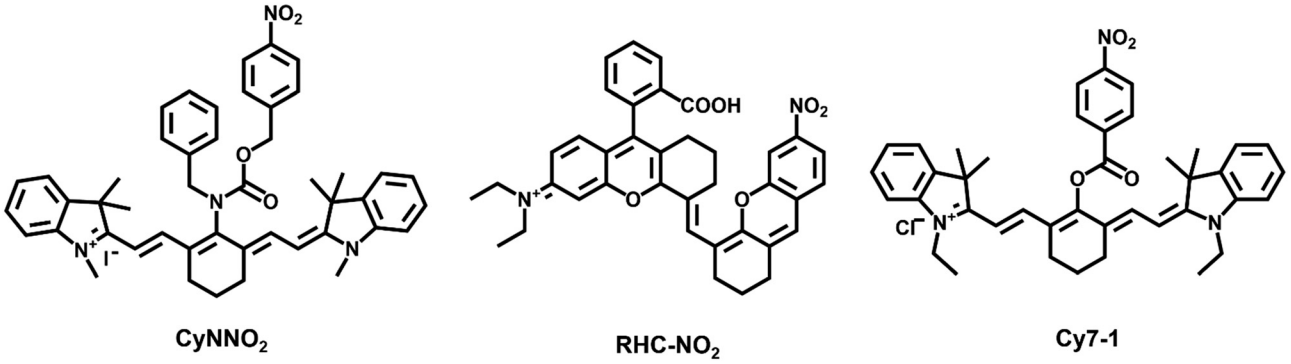

Fig. 1 The structures of fluorescent probes $CyNNO_2$, RHC-NO_2 and Cy7-1.

Chang *et al.* reported a near-infrared probe TiNIR (tumor-initiating cell probe with near-infrared) for tracking and inducing death of lung carcinoma tumor-initiating cells (TICs) by targeting HMOX2 (Fig. 2).[43] TiNIR λ_{max} of excitation = 805 nm and λ_{max} of emission = 825 nm. The probes had dual potential at different concentrations. The low-concentration of TiNIR (>1 μM, 24 hours) repeated injection of high-concentration (100 μM, 100 μL/10 g) probe into tumor mouse models, the TiNIR could specifically induce apoptosis of TICs. However, when sorting cells, the best concentration of TiNIR was 10–100 nM. The group verified the good performance of the probe in lung carcinoma cells and tumor-bearing mice. Moreover, it was confirmed that the probe could inhibit HMOX2 activity to induce ROS accumulation and tumor cell death.

Powis *et al.* designed and synthesized a fluorescent probe (TiY), which could be used to detect TICs when binding to vimentin.[44] TiY $\lambda_{ex.}$ = 553 nm and $\lambda_{em.}$ = 572 nm. TiY imaged TICs in many carcinomas. And at high concentrations, TiY also showed anti-TIC activity. This suggested that TiY might be an exceptional chemical tool for the visual surgical navigation of TICs.

Kim *et al.* designed and synthesized an NQO1-activatable near-infrared fluorescent probe (NIR-ASM).[45] The probe conjugated dicyanoisophorone (ASM) as the fluorophore and NQO1 substrate quinone propionic acid (QPA) as the targeting group. The probe turned "ON" after responding to NQO1 in malignant tissue. Compared with other probes for NQO1, NIR-ASM had a large Stokes shift (~186 nm) and its maximum emission wavelength was at 646 nm. The use of the probe could distinguish NQO1-expressing carcinoma cells from normal cells. When NQO1-positive (A549 cell line) and -negative (MDA-MB-231 cell line) tumors evolved in the same animal, only the A549 tumor mass displayed strong fluorescence of the NIR-ASM probe.

Beharry *et al.* also designed an NQO1 specific chemiluminescent probe 1 (Fig. 3).[46] Trimethyl-locked quinone was as a trigger moiety covalently which bound to a phenoxy dioxetane moiety *via* a *para*-aminobenzyl alcohol linker. The fluorescence signal was generated by the bioreduction of the quinone to the corresponding hydroquinone. In the NQO1-containing A549 lung carcinoma tumor-bearing mouse model, the probe was able to generate a fluorescence response. However, no fluorescence signal was observed in the NQO1 negative H596 lung carcinoma-bearing mouse model. It was confirmed that probe 1 could distinguish lung carcinoma types with different NQO1 activity levels.

Lin *et al.* designed and synthesized a small molecule photosensitizer (PS) that utilized the high levels of hNQO1 in carcinomas.[47] The probe was comprised of a quinone

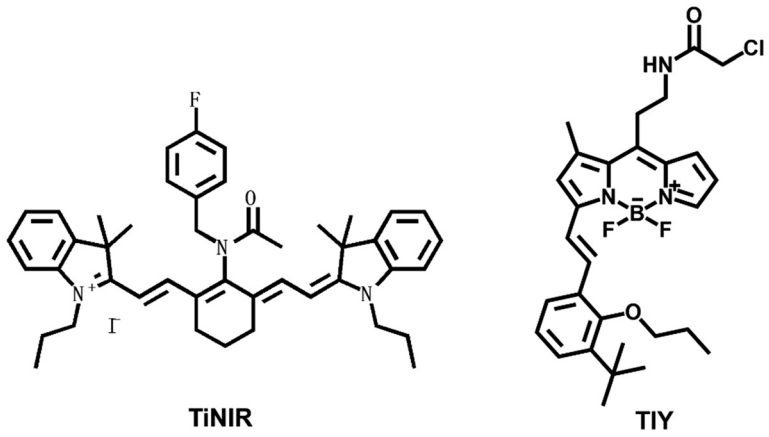

Fig. 2 The structures of fluorescent probes TiNIR and TiY.

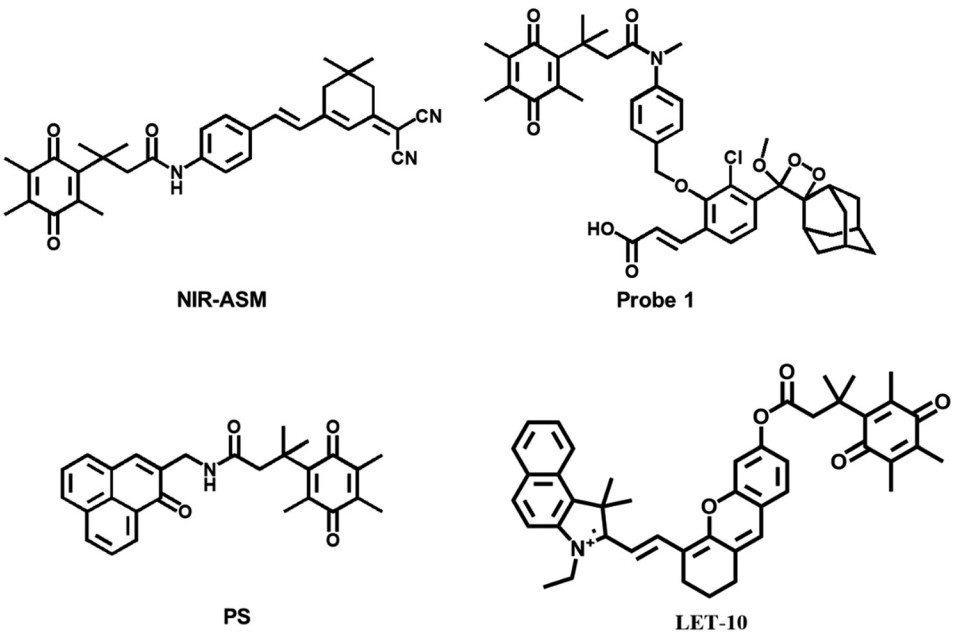

Fig. 3 The structures of fluorescent probes NIR-ASM, probe 1, PS, and LET-10.

substrate covalently linked through the central amide bond to phenalenone (PN). The quinone group quenched PN through photon-induced electron transfer (PET). A spontaneous intramolecular cyclization resulted from hNQO1-mediated reduction of quinone to a quinol. The reaction released dihydrocoumarin and the native PN, as well as the generation of cytotoxic singlet oxygen upon stimulation. A dose-dependent photocytotoxic response was observed in lung carcinoma cells (A549), which was not found in a common lung cell line (MRC9), demonstrating that the probe could be used for carcinoma-targeted therapy.

Yamashita *et al.* reported an activatable naphthalocyanine dye-based probe (LET-10) for near-infrared fluorescence/photoacoustic duplex imaging of hNQO1 in cells and *in vivo*.[48] Once hNQO1 (5 μg mL^{-1}) was detected within 10 min, the fluorescence intensities at 730 nm increased. The detection limit was 0.21 μg mL^{-1} for fluorescence imaging. The probe could be utilized to detect hNQO1-positive A549 tumor-bearing mice *via* tail vein injection.

Yang *et al.* designed and synthesized an HNE-responsive fluorescent probe F-1, which utilized dicyanoisophorone-containing (*E*)-2-(3-(4-aminostyryl)-5,5-dimethylcyclohex-2-en-1-yli dene) malononitrile (TMN-NH_2) as the fluorophore, and pentafluoroacetamide was selected as an HNE active trigger.[49] The fluorescence of TMN-NH_2 could be detected when F-1 reacted with HNE. Compared with the traditional fluorescent probe for detecting HNE, HNE was stable and hardly needed special storage conditions. The probe could track HNE in A549 cells with a large Stokes shift (182 nm) and a high sensitivity of limit of detection ~5.6 ng mL^{-1}.

Lin *et al.* constructed a fluorescent probe NEP, which was also used to detect HNE (Fig. 4).[50] The probe used pentafluoroethyl as the response group and hemocyanin dye as the fluorophore. There was more than 25 fold red fluorescence intensity when the probe reacted with NE. The long fluorescence emission wavelength ($\lambda_{em\ max}$ = 700 nm) of NEP allowed the direct detection of NE transport and uptake at the cellular level. These made the probe NEP a new tool for clinical diagnosis of lung diseases.

Since the early detection of the potential biomarker of lung carcinoma is crucial, Goldberg *et al.* synthesized a near-infrared fluorescence and photoacoustic duplex hemi-cyanine

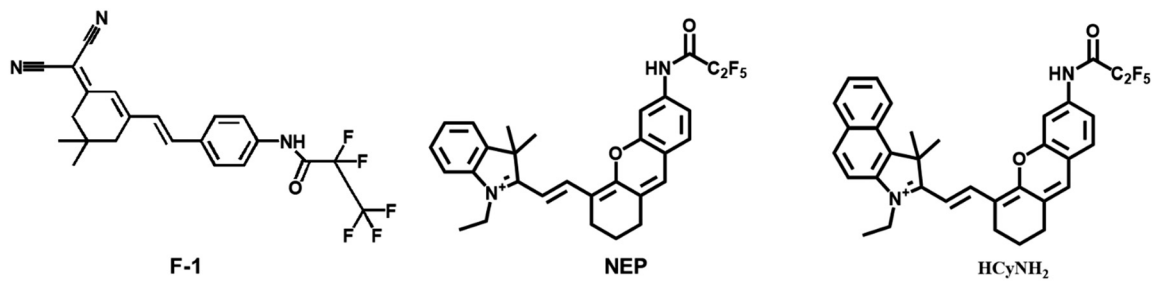

Fig. 4 The structures of fluorescent probes F-1, NEP, and $HCyNH_2$.

imaging probe ($HCyNH_2$) for monitoring of HNE.[51] The probe offers good selectivity and response ability to HNE. The fluorescence intensity is at 725 nm, and the limit of detection is 15.76 ng mL^{-1}. The probe can be used to real-time monitor HNE activity in the subcutaneous A549 xenograft model.

4. Probes based on small molecule ligands

Mammalian cells contain a variety of proteolytic systems, including the lysosomal system (cathepsins B, D, H, L, and other hydrolases), mitochondrial proteases, and the ubiquitin–proteasome pathway, among others.[52] The increase of proteolytic enzymes has been confirmed in many tumors. The increase of proteolytic enzymes may adapt to the rapid cell cycle and maintain tumor invasion, metastasis and angiogenesis. Umar Mahmood's group designed and synthesized a fluorescent probe, C-PGC, which was linked to a long-circulating graft copolymer consisting of poly-L-lysine and methoxy polyethylene glycol succinate.[53] The excitation and emission wavelengths of the probe were at 673 nm and 689 nm, respectively. After reaction with protease, the probe showed a strong fluorescence signal. Subsequently, the probe was used to lung carcinoma cell implanted mice for detection.[54] When probes were unquenched by several biologically relevant proteases that cleave lysine–lysine bonds, this would lead to a fluorescence increase with mouse thoracoscopy. The smallest pleural and subpleural lesions could be detected with the help of the probe, which might be a useful tool for staging or restaging lung carcinoma patients.

Strongin *et al.* constructed a probe for cathepsin-B, CyA-P-CyB, which contains two cyanine moieties (CyA and CyB), linked by a cathepsin B-activated peptide (Gly-Phe-Leu-Gly) (Fig. 5).[55] Cathepsin-B is one of the lysosomal proteases, which plays an important role in regulating carcinoma angiogenesis and invasion. Based on the fluorescence resonance energy transfer (FRET) mechanism, the probe consisted of a fluorescence donor CyA and a fluorescence quencher. After the peptide linker of the probe was interrupted by cathepsin B, the probe emitted strong NIR fluorescence. The final reaction product Cy–S–Ph–NH_2 had a photodynamic therapy effect and could produce severe phototoxicity to tumor cells at 808 nm. Thus, the probe had multiple merits, including specific near-infrared imaging, specific phototoxic efficacy on carcinoma cells, and phototherapeutic effects on tumor-bearing mice. These properties of the probe were confirmed in HeLa cells and H640 tumor-bearing mice.

Thioredoxin reductase enzyme (TrxR1) was overexpressed in cells aiding their growth and proliferation while inhibiting apoptosis. The levels of TrxR1 have been shown to directly correlate with the progression of human lung carcinoma. Peng *et al.* described the synthesis of a fluorescent probe 1a

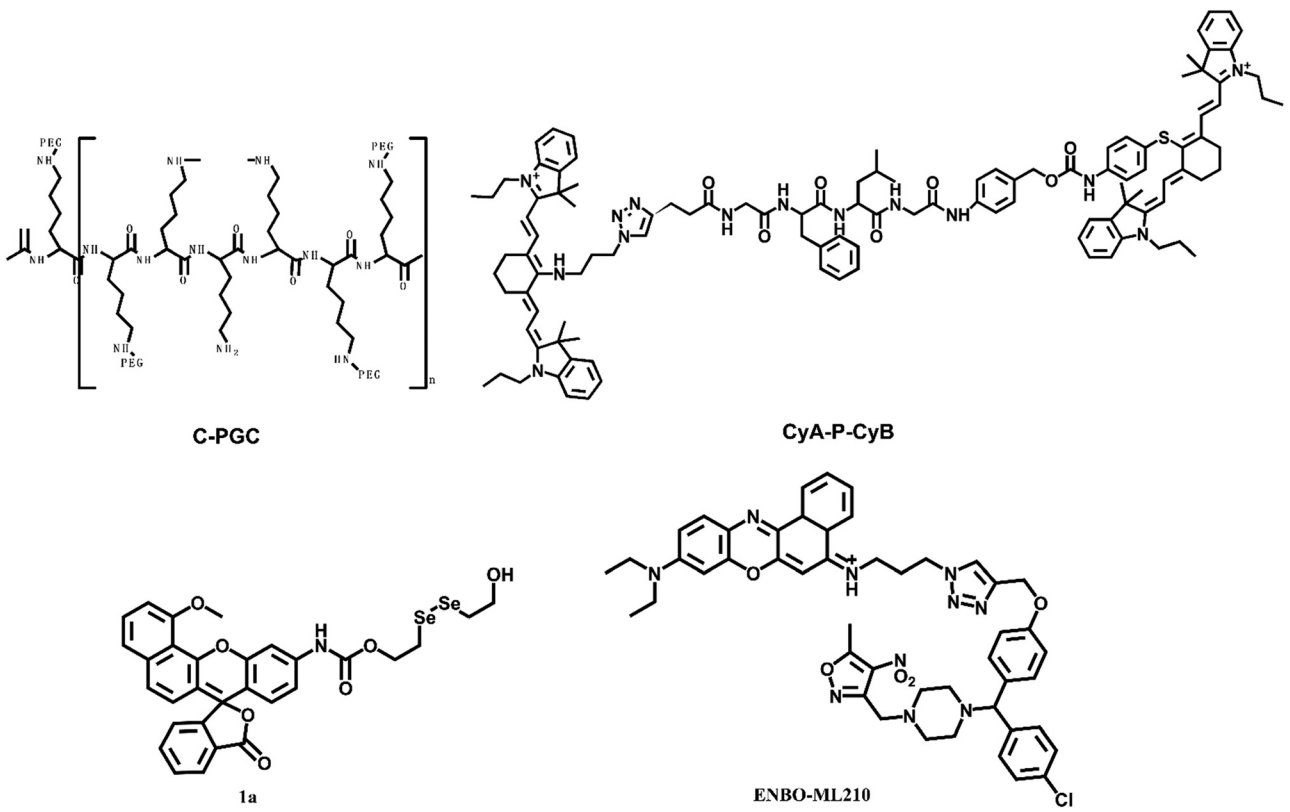

Fig. 5 The structures of fluorescent probes C-PGC, CyA-P-CyB, 1a, and ENBO-ML210.

for the evaluation of TrxR1 with a Michaelis–Menten constant (K_m) of 15.89 μM.[56] The cell imaging experiment confirmed that the diselenide probe could be used to indicate the TrxR activity.

Glutathione peroxidase 4 (GPX4) was overexpressed in non-small cell lung carcinoma (H1299) cells. Shi *et al.* synthesized a probe ENBO-ML210 through a simple "click" reaction between the fluorophore Nile blue and ligand ML210yne.[57] The fluorescence emission of the probe was within 600–700 nm. The results revealed that GPX4 is overexpressed in non-small cell lung carcinoma (H1299) cells.

Shi *et al.* designed and synthesized a heptamethine indocyanine dye IR-780 with absorption centered at 780 nm, which can be easily detected by an NIR fluorescence detection system (Fig. 6).[58] It preferentially accumulated in the mitochondria of drug-resistant human lung carcinoma cells (A549/DR) selectively and inhibited cell growth, self-renewal, and metastasis. IR-780 could destroy the mitochondrial function to induce apoptosis of A549/DR cells. IR-780 also indicated significant antitumor activity and inhibited carcinoma recurrence in treating the Lewis lung carcinoma tumor-bearing mouse model.

Caspases (cysteine Asp-specific proteases) play crucial roles in cell apoptosis. Lv *et al.* designed a fluorescent probe (DEVD-TPE) for investigating caspase-3 in living cells using the principle of aggregation-induced emission (AIE).[59] DEVD-TPE was composed of the substrate peptide Asp-Glu-Val-Asp (DEVD) and the AIE fluorophore tetraphenylethene (TPE). In a weak alkaline solution, the probe DEVD-TPE emitted almost no fluorescence because of the dynamic rotation of the phenyl rings in solution. The aggregation of TPE led to enhanced fluorescence emission, when the fluorescence response group TPE was cleaved by caspase-3. Thus, DEVD-TPE could be used for the rapid sensing of caspase-3 in living cells, which suggested the potential of the AIE probe DEVD-TPE for the rapid detection of non-small cell lung carcinoma.

Cysteine (Cys) is one of the basic nutritional amino acids in normal physiological processes. However, abnormal levels of intracellular Cys will result in many diseases, such as carcinoma. Yu *et al.* designed a ratiometric fluorescent probe Cy-OAcr for the detection of Cys in mitochondria (Fig. 7).[60] Probe λ_{ex} = 750 nm, λ_{ex} = 535 nm. The fluorescence ratio signal ($F_{Ratio} = F_{635\ nm}/F_{794\ nm}$) of Cy-OAcr could reveal the level changes of Cys. Cy-OAcr involved a lipophilic iminium cation moiety, which served as the mitochondrial targeting group, and an acrylate group, which served as the Cys recognition switch, as well as a fluorescence regulator for rearranging the conjugated π-electron molecular structure of the cyanine fluorophore. Once Cys level changes were detected, there emerged an absorption and fluorescence spectral blue shift, which was appropriately beneficial to ratiometric fluorescence detection. The probe has been used to evaluate the cysteine levels in an orthotopic lung carcinoma model and to distinguish carcinoma tissues from normal tissues.

Chan's group designed a live cell tracking biological probe targeting lysosomes, Cy-Lyso.[61] The probe could achieve targeted aggregation that was independent of the lysosomal acidic environment. Cy-Lyso contained two moieties: near-infrared cyanine fluorophore and *p*-fluorobenzenesulfonyl recognition unit. The *p*-fluorobenzenesulfonyl group could be utilized as a lysosome targeted guider. After the cyanine dye

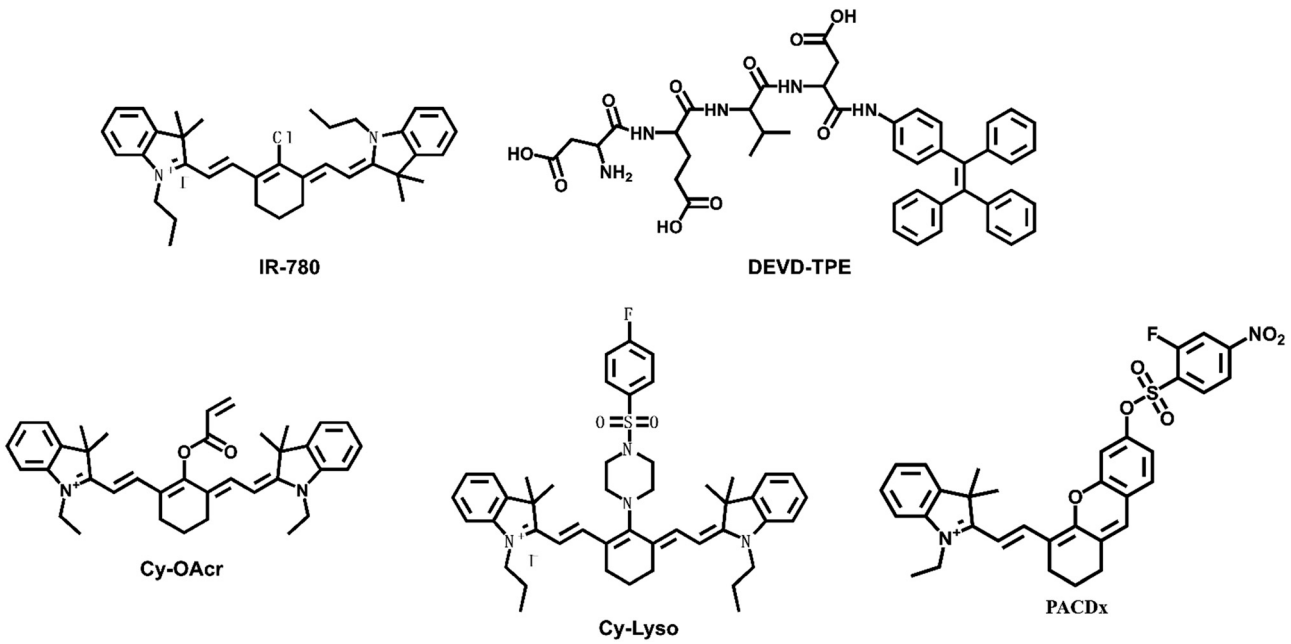

Fig. 6 The structures of fluorescent probes IR-780, DEVD-TPE, Cy-OAcr, Cy-Lyso, and PACDx.

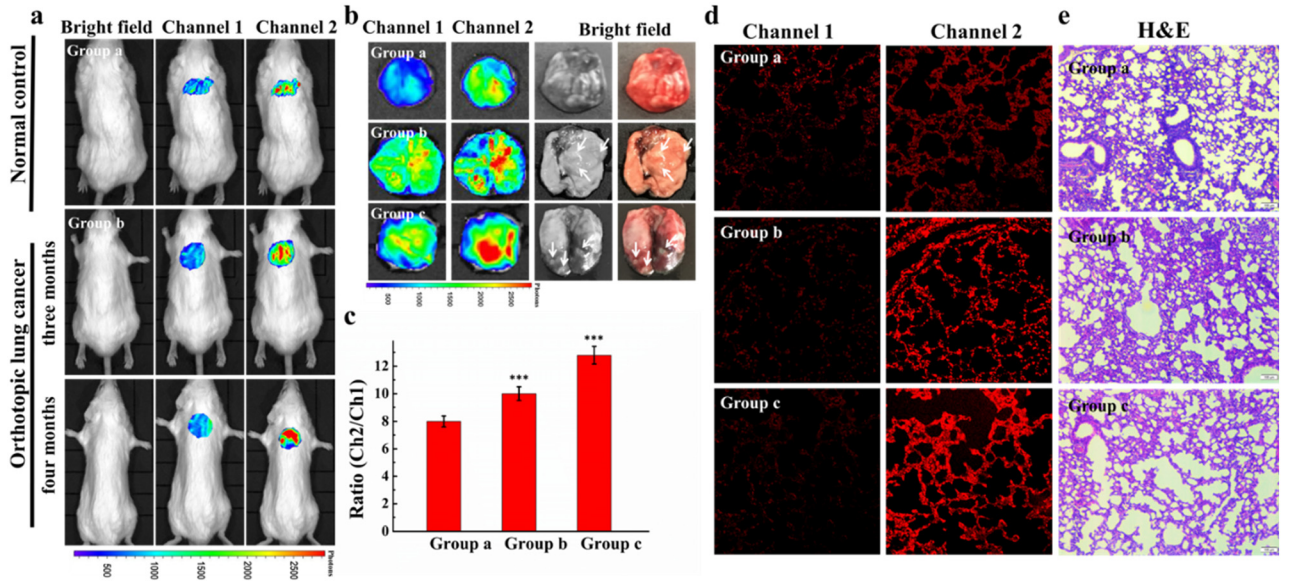

Fig. 7 Small animal fluorescence imaging of Cys in orthotopic lung carcinoma mice. a) Probe images of Cys in mice. b) *Ex vivo* fluorescence imaging of lung carcinoma. c) The average ratio intensity values of mouse groups a–c within 30 min. Ratio values in c). d) Confocal fluorescence images of fresh lung tissue slices in mouse groups a–c. e) H&E stained lung tissues from normal tissues and carcinoma lesions in groups a–c. Reproduced with permission from ref. 59, Copyright 2020 Elsevier.

was attached to the *p*-fluorobenzenesulfonyl group, the targeting transition of the probe from mitochondria to lysosomes could be achieved, resulting in long-lasting fluorescence in living cells. Cy-Lyso could be utilized to track the metastasis of lung carcinoma cells.

Glutathione (GSH) is also a potential small-molecule target for distinguishing between normal and pathological states. Golding *et al.* reported a photoacoustic imaging-based probe (PACDx) for the selective detection of elevated glutathione (GSH) in lung carcinoma.[62] Under physiological conditions, the probe could give a dose-dependent signal increase when PACDx was incubated with 10 mM GSH for 1 h. Upon detection of elevated GSH in an orthotopic lung carcinoma model, the signal ratio in the tumour region was 3.17 ± 0.91.

5. Probes as photodynamic therapy for lung carcinoma

From 3000–4000 years ago, people have taken advantage of sunlight for the treatment of skin diseases. In 1895, Niels Ryberg Finsen established the system of modern light for phototherapy of lupus as a therapeutic tool.[63] Photodynamic therapy (PDT) has become an efficacious therapy method for various malignant carcinomas. The treatment principle of PDT is to utilize the photochemical interaction of a certain light source, a suitable photosensitizer, and molecular oxygen for producing reactive oxygen species which leads to cell death.[64] Up to now, photosensitizers have the advantages of low phototoxicity to healthy cells, specific localization into tumor cells, a higher level of singlet oxygen production, a better stable molecular structure, and a higher light attenuation rate.[65] Compared with traditional radiotherapy and chemotherapy, PDT has many advantages. PDT can avoid serious adverse reactions and treat inoperable carcinoma parts. Besides, PDT can also treat the lesions, so the other parts of the body will not be exposed to phototoxicity.[66]

As a minimally invasive tumor therapy, PDT has been used to treat lung carcinoma as early as 30 years ago and has gradually attracted attention.[67,68] At present, several photosensitizers have been approved by the US Food and Drug Administration (FDA), for instance, talaporfin/NPe6, temoporfin, methyl-aminolevulinate (MAL), porfimer sodium (Photofrin), and [1-hexyloxyethyl]-2-devinyl pyropheophorbide-a (HPPH).[66] Photofrin is the most common exploited PS for the treatment of lung carcinoma. At present, there are many cases of successful PDT application in the lung carcinoma treatment. Horinouchi's group started a phase II clinical trial on the effect of Photofrin for early-stage lung carcinoma.[69] In 2003, Cui's group published a phase II clinical trial on the effect and safety of photodynamic therapy for early-stage lung carcinoma with NPe6.[70]

Yuan's group injected hematoporphyrin injection Hiporfin into 20 patients with diagnosed lung carcinoma.[71] After receiving photodynamic therapy for 3 months, the patients were relieved with the shrinking of the tumor volume (Fig. 8). Given the good therapeutic effect achieved in the early stage of photodynamic therapy, many scientists focus on the development of new photodynamic therapy reagents, such as classical cyanines, squaraines, porphyrins, phthalocyanines and their derivatives.[72]

Chakravarty's group designed and synthesized an NIR heptamethine dye, IR-808 (Fig. 9).[73] IR-808 hardly required

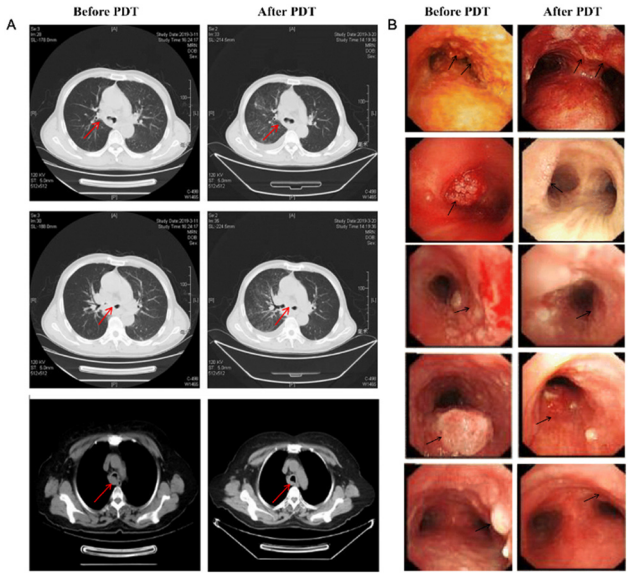

Fig. 8 (A) CT image changes in the chest after PDT treatment 3 months later. (B) CT image changes in bronchoscopy after PDT treatment 3 months later. Reproduced with permission from ref. 70, Copyright 2020 Spring Nature.

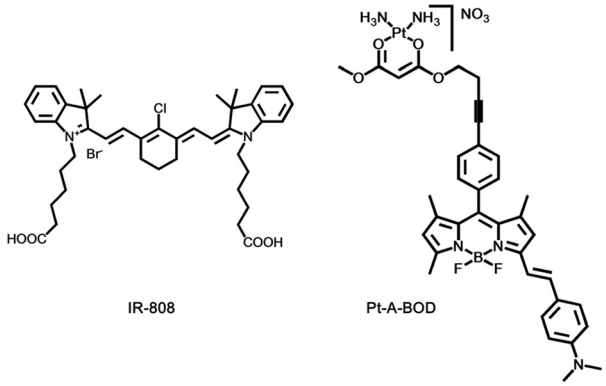

Fig. 9 The structures of fluorescent probes IR-808 and Pt-A-BOD.

chemical conjugation to tumor-specific ligands or photosensitizers, owing to the preferential tumor accumulation and photosensitization properties. In serum, the absorption peak of IR-808 was at 740 nm and the fluorescence emission peak was centred at 825 nm. The IR-808 incubation of rTDMC, HeLa, or LLC tumor cells showed dose-dependent photosensitizing effects. After two doses of photodynamic therapy, the LLC tumor xenograft model of the IR-808 PDT group showed significant tumor inhibition.

Choyke's group presented a platinum(II) complex, $[Pt(A\text{-}BOD)(NH_3)_2](NO_3)$(Pt-A-BOD). The probe had a red-light activatable BODIPY fluorophore that could switch on an active platinum(II) species release for chemotherapeutic action once PDT activity is initiated involving the monostyryl BODIPY fluorophore through red light.[74] Pt-A-BOD could rapidly accumulate in the mitochondria of A549 cells, resulting in apoptosis with the generation of singlet oxygen.

6. Near infrared probes as photoimmunotherapy for lung carcinoma

Near-infrared photoimmunotherapy (NIR-PIT) is a new kind of carcinoma therapy method, which generally includes a tumor-targeting specific monoclonal antibody (mAb) and a photoabsorber through a linker, which is also known as an antibody–photosensitizer conjugate (APC).[75] The target cells are destroyed by NIR light irradiation inducing highly selective immunogenic cell death while the normal adjacent cells remain intact. PIT is distinct in combining the essential benefits of antibody-mediated tumor cell targeting to realize high tumor specificity and laser-activated biophysical strategies to precisely cause rapid carcinoma cell death.[76]

The first phase I clinical trial of NIR-PIT was to inject an antibody–photoabsorber (IR700) conjugate (APC) and RM1929 into the carcinoma tissue of patients with head and neck tumors.[77] The tumor was exposed to NIR light at 690 nm wavelength for 24 h for the purpose of treatment. Dylla's group used IR700 to conjugate with panitumumab (an antibody targeting EGFR) to form a photoabsorber, IRDye700DX, which was utilized in the treatment of a mouse model of transgenic lung carcinoma.[78] During the treatment period, the tumor volume decreased gradually under the observation of MRI (Fig. 10).

Small cell lung carcinoma (SCLC) is characterized by low prognosis and limited treatment options. Delta-likeprotein3 (DLL3) is specifically expressed in SCLC, therefore, it has been considered to be a desirable therapeutic target for SCLC patients.[79] Rovalpituzumab tesirine (Rova-T) was the first antibody–drug conjugate targeting DLL3. Hasegawa's group designed a near-infrared photoimmune reagent targeting DLL3 for the treatment of SCLC.[80] The anti-DLL3 monoclonal antibody rovalpituzumab was linked with the photosensitizer IR700 to yield a molecular targeting reagent, Rova-IR700. When Rova-IR700 was injected into tumor-bearing mice intravenously, it could be observed that Rova-IR700 only accumulated in the carcinoma tissues, and the carcinoma tissues shrank after light exposure significantly.

Malignant pleural mesothelioma (MPM) has been known as a progressive thoracic malignancy arising from pleural mesothelial cells and subpleural stroma. Kobayashi's research has designed a targeting agent NZ-1-IR700 for the treatment of MPM.[81] NZ-1 is an anti-human PDPN antibody, conjugated with an IR700 NHS ester as a photosensitizer. By repeated near-infrared light irradiation, it was confirmed that NZ-1-IR700 could have an antitumor effect on an orthotopic MPM mouse model. Pleural metastasis of lung carcinoma is common in patients with advanced thoracic carcinoma, but it is difficult to be well controlled, and the prognosis is often poor. Kobayashi's group reported an APC composed of trastuzumab and a phthalocyanine dye, IRDye-700D.[82] The results showed that pleural metastasis was reduced significantly after the NIR-PIT treatment. The effect of NIR-

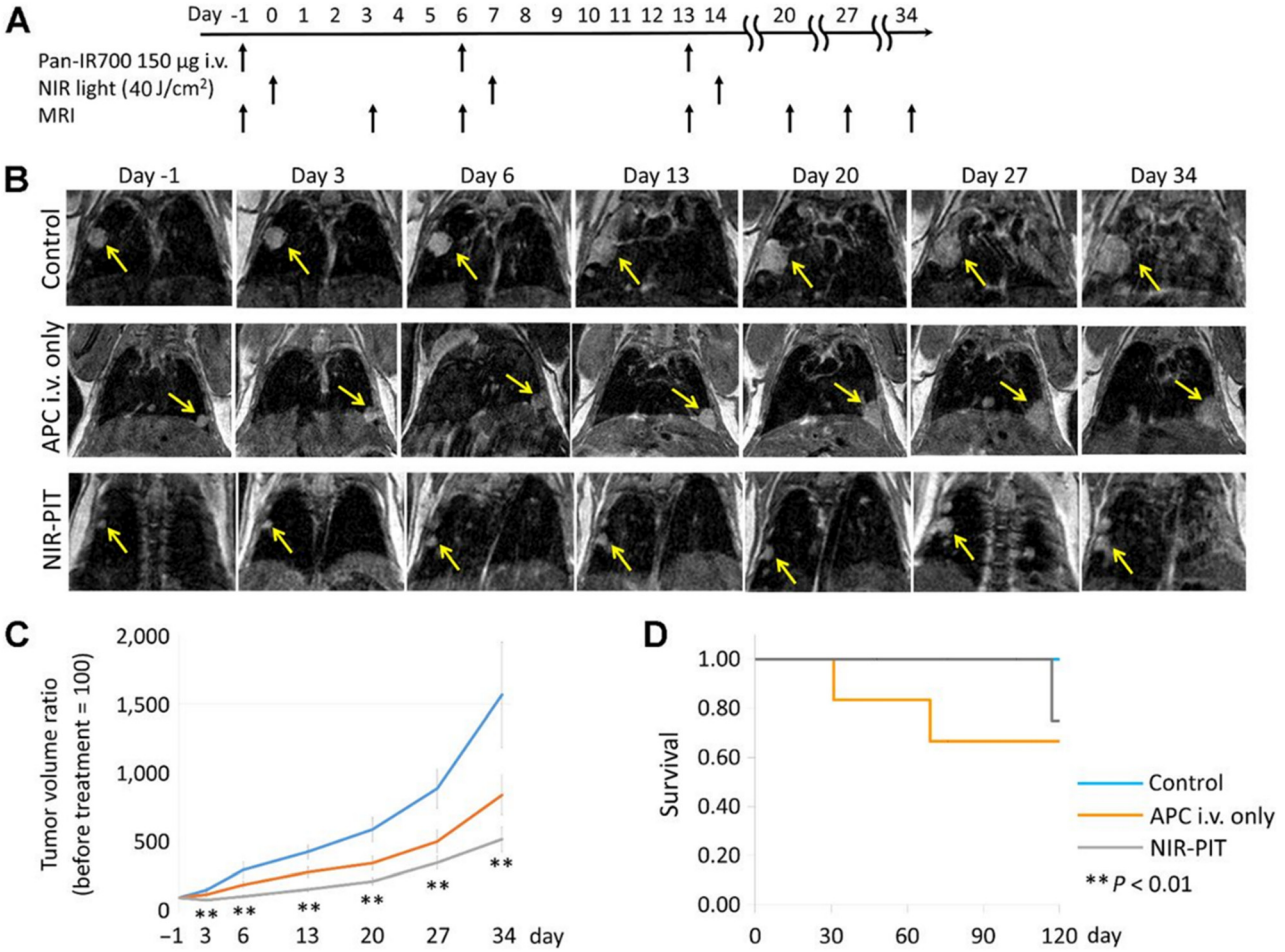

Fig. 10 *In vivo* effects of probe NIR-PIT on the mouse model of lung tumor. (A) NIR-PIT regimen of APC administration and exposure to near-infrared light. MIR images were acquired at the corresponding time points. (B) MIR images of the lung tumor bearing mouse model. The measured size of the lung tumors of the animals developed rapidly in the control group and APC i.v. only groups, whereas the measured size of the lung tumors developed only gradually in the NIR-PIT group. (C) The tumor volume ratio was suppressed considerably in the NIR-PIT group compared to the control group, while there was no obvious discrimination in the tumor volume ratio in the APC i.v. only group compared to the control group. (D) The experimental results showed that there was no evident difference in the survival rate of the three groups of mice. Reproduced with permission from ref. 77, Copyright 2017 American Association for Cancer Research.

PIT on the metastatic pleural disease was also confirmed by fluoroscopic thoracoscopy.

NIR-PIT is a promising treatment for pleural metastatic tumours. Although NIR-PIT is effective in a variety of tumour models, the limitation of NIR-PIT is that it is difficult to deliver NIR light to the deeply located tumours. Thus, it is more advantageous for the lungs and thoracic cavity, which are more gas-filled organs. Therefore, how to overcome this shortcoming is also the focus of future research.

7. Lung carcinoma clinical therapy with fluorescence-guided surgery

Fluorescence-guided surgery (FGS) is a type of fluorescence clinical bioimaging technology, in which a certain fluorescent probe is injected into the patient before or during surgery.[24] The targeting fluorescent probe can accumulate into the lesion and then displays specific fluorescence imaging. The fluorescent reagent can help to distinguish the normal tissue and diseased tissue, which can assist the clinicians to remove the diseased part within a safe range accurately.[83] Fluorescence clinical bioimaging technology is characterized by simple operation, high resolution, good safety, and *in situ* and real-time, as well as targeted monitoring. In recent years, it has been considered to have broad application prospects in clinical surgical navigation, especially in lymph node and tumor biopsies. At present, there are several near-infrared fluorescent dyes approved for clinical utilization, such as sodium fluorescein, indocyanine green (ICG), methylene blue (MB), and 5-aminolevulinic acid (5-ALA).[84] There are also some probes, such as BLZ-100, LUM015, OTL38, and SGM-101 approved in clinical trials.[85–88] There are also new fluorescent probes in preclinical experiments, such as zwitterionic NIR fluorophores and monoclonal antibody-based fluorescent probes.[89,90] Although some new fluorescent agents have not been used in the clinical application, there is

a high benefit in the development and promotion. According to the research progress of FGS related to pulmonary lesions in recent years, the aspects of fluorescent reagents, sentinel lymph node (SLN) detection, pulmonary bullae, pulmonary nodules, solid tumor resection, and pleural diseases will be described respectively.

The fluorescent probe plays an important role in FGS. The fluorescent probe can distinguish the lesion from the surrounding tissue, so the clinicians can find the tumor tissue during the operation. The fluorescent agents can be divided into intrinsic and extrinsic probes.[24] The intrinsic probes mainly refer to naturally occurring fluorophores, for example aromatic amino acids, porphyrins, and flavins in the body, and other fluorophores in the natural environment, for instance the green fluorescent protein (GFP) found in the jellyfish and the chlorophyll in plants.[91,92] One of the main merits of intrinsic fluorophores for FGS is that they can be studied without changing cells or structures. But there are also higher requirements for tissue depth, excitation and emission spectra, and imaging time. Therefore, there are more extrinsic probes being developed.[93] The extrinsic probes refer to the agents that are designed and synthesized to emit fluorescence under specific pathophysiological conditions or even at specific locations. However, if the extrinsic probes are used in medicine, they must meet strict regulatory requirements before they can be approved. Therefore, there are only a few fluorescent probes that can be employed in clinical practice so far. The following section will focus on the fluorescent probes that are approved by FDA and their clinical application in lung diseases.

7.1 Lung carcinoma clinical imaging probes

Fluorescein sodium (FL) was synthesized by Adolf von Baeyer in 1871, with the fluorescence peak excitation centered at 490 nm and fluorescence emission centered at 510 nm, respectively.[94] It is one of the first fluorescent dyes approved by the FDA. After FL is injected into the body, it will not cause any serious adverse reactions and can be quickly excreted. Fluorescein sodium is inexpensive, and the fluorescence can be observed with the naked eye, so it has been widely used in clinical practice since its discovery. The first application of FL in humans dates back to 1946. For a patient with gastric carcinoma who underwent laparotomy, FL injections were used to distinguish diseased and normal tissues. It was first used in surgery for brain tumor identification in 1948 and is still widely used in neurosurgery to identify various types of brain tumors.[95,96] FL has also been used in ophthalmic surgery since the 1990s and is still widely used in clinical fundus angiography.[97] FL has been more and more used and studied in the clinic, such as in the detection of oral dysplasia and oral carcinoma, helping to judge dural arteriovenous fistulas and study pharmacokinetics.[98–100] However, the spectrum of FL is in the visible range, resulting in its fluorescence overlapping with the fluorescence of many endogenous fluorophores.

Indocyanine green (ICG) is also an FDA-approved near-infrared fluorophore for clinical application, with a history of more than 50 years of applied research. ICG is a water-soluble heptacarbocyanine fluorophore with an excitation peak at 780 nm and an emission peak at 830 nm, respectively.[101] The ICG fluorophore was developed by Kodak in 1955 for near-infrared photography and was approved for monitoring cardiac output a few years later. Since then, ICG has been widely used in the medical field, mainly in cardiology, ophthalmology and angiography.[102–104] The current clinical research focuses on carcinoma surgery, sentinel lymph node detection, and detection of leakage in some procedures. ICG is the most suitable near-infrared photosensitizer so far, but it has disadvantages such as low fluorescence quantum yield, quick metabolism time, and photodegradation, which seriously limit the wide application of ICG in PDT and photothermal therapy.[105] In the nano-medical field, ICG is also widely used in the loading of nanoparticles.[106] Indocyanine green has a relatively favorable circulating half-life and can selectively accumulate in or around lesions, making it a preferential contrast agent for surgical navigation.[107,108]

As a precursor of protoporphyrin IX (PpIX), 5-aminolevulinic acid (5-ALA) is used in the biosynthesis of heme.[24,109] Because it is naturally present in the human body, it is less biologically toxic than any other extrinsic probes. The fluorescence excitation and emission are centered at 410 nm and 630/700 nm, respectively.[24] PpIX accumulates in malignant cells such as melanoma, breast carcinoma, malignant glioma tissue and lung carcinoma. The current literature mainly focuses on the application in glioma surgery. In 2017, 5-ALA also received FDA approval for imaging high-grade gliomas. The exogenous 5-ALA can smoothly penetrate the blood–brain barrier and enter the brain tissue, enabling fluorescence visualization of brain tumors.[109] Besides, some researchers use 5-ALA to achieve the purpose of PDT therapy and nanoparticle targeted therapy.[110–112]

Methylene blue is also a well-known fluorescent probe that absorbs wavelengths from 550 to 700 nm (Fig. 11).[24] MB can be excreted *via* organs, such as the liver and kidneys, and it is suitable for imaging the biliary tract and ureter. Some researchers also used CT-guided injection of methylene blue/collagen into pulmonary nodules, and then performed thoracoscopy.[113] The results showed that all pulmonary nodules could be displayed during surgery and negative margins could be achieved. This provides a safe and efficient technique for thoracoscopic pulmonary nodule resection.

7.2 Lymph node mapping for lung carcinoma

The lymphatic system is distributed in all parts of the body. It is composed of lymphatic vessels, lymph nodes, and central lymphoid organs. It plays a crucial role in the immune system of the human body. The sentinel lymph nodes (SLNs) are the first lymph nodes in which tumor cells

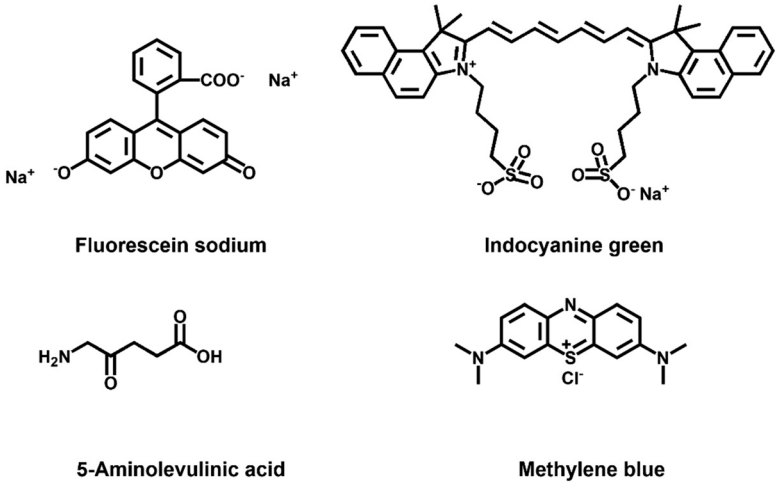

Fig. 11 The structures of lung carcinoma clinical imaging probes.

from the primary site are most likely to spread.[114] The sentinel lymph nodes serve as a barrier to prevent carcinoma cells from spreading from the lymphatics. The SLN results can help guide clinicians to judge whether malignant tumors have lymph node metastasis.[115] For lung carcinoma, lobectomy combined with extensive lymph node dissection is now the golden standard of therapy for lung carcinoma in thoracic surgery, but some experts point out that for some patients, especially those with poor lung function, segmentectomy combined with limited lymph node dissection is sufficient. There are many clinical methods for intraoperative detection of SLNs, but they all have certain limitations. The non-invasive lymph node monitoring methods have also been lacking in clinical practice. Therefore, many researchers turn their attention to fluorescence imaging.[116] Fluorescence angiography of lymph nodes has gradually become a popular diagnostic imaging method. It has been developed and researched by multiple research groups for clinical use. ICG is one of the most commonly used contrast agents. Yolonda L. Colson's group studied whether the dose of ICG affects the detection rate of SLNs.[117] 3.8 mg to 2500 mg ICG has been injected around the tumor in patients with suspected stage I/II NSCLC, and then the patients underwent thoracotomy or thoracoscopic surgery. The results displayed that less than 25% of SLNs were detected in the 600 mg or less dose group, while the 1000 mg or greater dose group detected an 89% success rate. And the presence of metastasis was demonstrated in the subsequent histological analysis. Subsequently, the group performed an intraoperative biopsy and ICG peritumoral injection in suspected or known stage I NSCLC patients under bronchoscopy.[118] 12 patients underwent bronchoscopy-guided labeling of lung lesions with ICG. The pathological examination of the lesions marked by ICG indicated that 10 patients were diagnosed with NSCLC, and 8 of these 10 patients had positive sentinel lymph nodes. And the patients had no obvious adverse reactions after injection of ICG, so bronchoscopy-navigated near-infrared lesion localization and SLN identification are safe and feasible.[119] Rapid identification of metastatic mediastinal lymph nodes has also become an urgent challenge in lung carcinoma surgery. Wang's group established 32 lung squamous cell carcinoma mediastinal lymphatic metastasis SCID-CB17 mice with Ma44.3 cells. 1.25 ml kg^{-1} ICG (1.25×10^{-2} mg ml^{-1}) was injected into the mice intratracheally, and then the fluorescence changes were observed at four different times.[120] The results showed that ICG had the strongest fluorescence signal at 2 to 4 h. But at 0.5 h and 2 h, ICG fluorescence reflected the mediastinal metastasis of lymph nodes. Using ICG to image lymph nodes can achieve accurate localization and lymph node staging in early-stage lung carcinoma. However, how ICG reaches metastatic mediastinal lymph nodes remains unclear and requires further study.

7.3 Pulmonary bullous lesion detection in lung carcinoma

Bullectomy under video-assisted thoracoscopic surgery (VATS) is considered to be the intervention of choice for most patients with spontaneous pneumothorax. However, some studies have shown that this measure has a higher recurrence rate, mainly because there are still residual bullous lesions that have not been completely removed. In order to better identify bullous lesions during surgery, Weichert's group conducted an experiment.[121] In this experiment, patients with spontaneous pneumothorax first underwent thoracoscopic exploration under visible light conditions. Then ICG (0.6 mg kg^{-1}) was injected intravenously, and the fluorescence state after pulmonary injection of ICG was observed in NIR mode (Fig. 12). Fluorescence was detectable in the lungs 10.5 s after ICG bolus (average 10–11 s), and the fluorescence density of bullous lesions was evidently lower than that of adjacent normal lung tissue. All excised lesions were confirmed to be bullous changes by pathology. This suggests that this technique has the potential to be widely used in VATS bullectomy in the future.

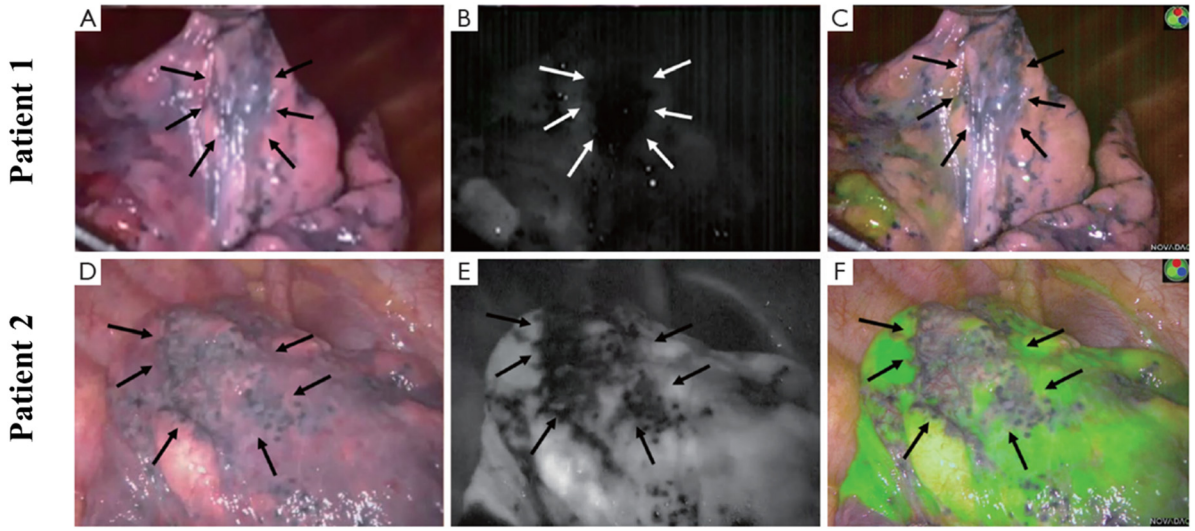

Fig. 12 Bullous lesions illustrated using a near-infrared thoracoscope. (A) The image of bullous lesion under white light; (B) the image of bullous lesion for fluorescence emission with 0.2 mg kg^{-1} ICG; (C) the syncretic mode of bullous lesion; (D) the image of bullous lesion under white light; (E) the image of bullous lesion for fluorescence emission with 0.6 mg kg^{-1} ICG; (F) the syncretic mode near bullous lesion. Reproduced with permission from ref. 120, Copyright 2016 *Journal of Thoracic Disease*.

7.4 Pulmonary nodule identification in lung carcinoma

The complete tumor resection is the most significant factor for the survival of lung carcinoma patients. However, the current surgical procedures are lacking high-sensitivity intraoperative image guidance, resulting in the inability to detect tiny tumors. The *in situ* and real-time near-infrared fluorescence bio-imaging technology serves as a powerful tool for recognizing lung nodules, surgical margins, and more.[122] In 2017, Singhal's group reported a case in which a folate receptor-targeted, near-infrared optical contrast agent (OTL38) was intravenously injected into a patient with suspected lung carcinoma before surgery.[123] OTL38 was excited at a wavelength of 774 to 775 nm with emission wavelengths from 794 to 796 nm. Intraoperatively, the suspected lesion showed high fluorescence intensity, and the frozen section of the lesion showed invasive lung adenocarcinoma. The final pathology confirmed the expression of folate receptor-α. The surgeons changed the scheduled lobectomy to remove the lesion with wedge resection. After a one-year follow-up, the patient showed no lung adenocarcinoma recurrence or drug toxicity. This case successfully utilized the targeting near-infrared intraoperative molecular fluorescence probes for surgical guidance of thoracic malignancies. Yu's group also employed near-infrared intraoperative probe to apply a folic acid-targeted contrast agent (OTL0038) to localization, lymph node sampling, and margin evaluation of primary lung adenocarcinoma.[124] The group injected OTL0038 intravenously into 10 dogs with lung carcinoma, and then performed thoracoscopy or thoracotomy for tumor resection. The researchers used near-infrared imaging equipment to image lung tissue *ex vivo* and *in vivo*. If the wound bed had residual fluorescence, the margins were considered positive. The group later used OTL0038 to conduct studies on 3 human patients. The results showed that *in situ* fluorescence could be detected in all tumors in dogs, and the sites with residual fluorescence at the tumor edge were pathologically confirmed to be malignant. The positive lymph nodes were also found using near-infrared imaging. The human studies confirmed that the fluorescence can be seen in the tumor site, and postoperative pathology examination confirmed lung adenocarcinoma (Fig. 13). There is no recurrence trend during follow-up.

Tian's group recruited 30 patients with early-stage lung carcinoma having peripheral nodules less than 2 cm.[125] The patients were injected with 100 to 150 ml of diluted ICG near the nodules under CT guidance to localize the nodules by observing ICG fluorescence using near-infrared thoracoscopy. The VATS resection was administrated to remove the lesion. The results showed that ICG fluorescence was clearly found in all 30 patients. The pathological results of surgical margins were negative, and 30 cases of primary lung carcinoma were finally diagnosed.

Chao's group recruited 36 patients with pulmonary nodules who received ICG *via* peripheral intravenous injection 24 hours before surgery and then underwent near-infrared fluorescence imaging thoracoscopic surgery.[126] During the operation, the traditional white light thoracoscopy was performed, followed by ICG fluorescence-guided exploration. The ICG fluorescence imaging detected 68 nodules during *in vivo* surgical navigation. However, 9 additional nodules were missed by conventional detection in 7 patients. Four of these nine nodules were identified as malignant or atypical adenomatous hyperplasia. The results of these studies further support the use of NIR contrast media for thoracoscopic surgery for the study of early-stage lung carcinoma. Choi's research group and Choia's research group also carried out related experiments, which further confirmed the feasibility of FGS.[127,128]

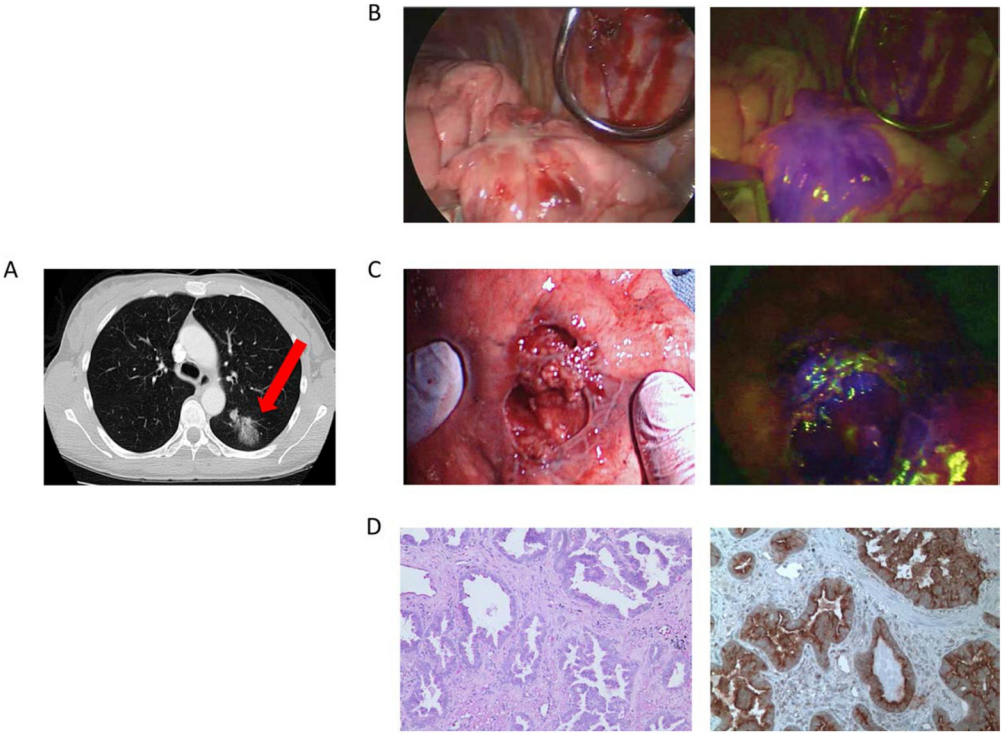

Fig. 13 The clinical case was a 55-year-old female. (A) Preoperative chest imaging revealed a mass in the left lower lobe; (B) white light navigation image and near-infrared fluorescence navigation image of the lesion obtained during surgery; (C) white light navigation image and near-infrared fluorescence navigation image of the lesion after operation; (D) pathological section verified an invasive adenocarcinoma. H&E staining and immunohistochemistry illustrated a strong folate receptor staining. Reproduced with permission from ref. 123, Copyright 2016 American Cancer Society.

7.5 Diagnosis and treatment of pleural disease

The local recurrence has been the Achilles heel of carcinoma surgery, and multiple examinations have shown that the complete resection of the tumor tissue is important for improving 5-year survival. The complete resection during surgery for malignant pleural mesothelioma is particularly difficult, owing to the technical difficulties of pleurectomy/cortectomy and extrapleural pneumonectomy and the occult feature of carcinoma itself. Therefore, Lv's group conducted a study of 8 patients with biopsy-proven epithelial malignant pleural mesothelioma, each of whom received 5 mg kg^{-1} ICG intravenously 24 h before tumor resection.[129] The tumor fluorescence was detected intraoperatively using near-infrared imaging equipment (Fig. 14). After the routine surgery complete resection of the tumor with the traditional standard, the surgical site is fluorescently imaged. When the residual fluorescence is detected, the additional tissue will be excised, and the specimen will be sent for pathological correlation. The final pathological diagnosis was mesothelioma. The technique has the potential to be used to improve outcomes for patients with mesothelioma.

7.6 Lung carcinoma diagnosis and therapy

Non-small cell lung carcinoma (NSCLC) seriously threatens human health and causes high mortality. The therapy of NSCLC is facing enormous challenges because of drug resistance and poor prognosis. The targeting drug delivery systems which are equipped with carcinoma cell specific small molecule ligands are considered to ameliorate the prognosis of carcinomas, because these drug delivery systems can facilitate antitumor drug accumulation into carcinoma lesions and leave healthy tissue unaffected. The optional imaging modality for pharmacokinetic tests basically depends on the concrete issue to be addressed. Yu's group designed and synthesized two new prodrugs (PPG and PBG) conjugating different targeting ligands for the therapy of NSCLC (Fig. 15).[130] The corresponding fluorescent navigator TPG was applied for EGFR-mutation resistance NSCLC. The therapeutic drug still used conditional gefitinib. The targeting unit was the novel polyamine analogue (PA) and GSH-responding disulfide bond. Azo-BODIPY was employed as the fluorescent unit for imaging and tracing drug release. PA was used not only for the carcinoma cell targeting, but also for the inhibition of the Akt pathway, which was the key survival mechanism of EGFR-mutation resistance NSCLC. TPG showed a superior therapeutic effect for the PC9 and H1650 cell-bearing mouse model (Fig. 16). Compared with the single gefitinib, the tumor volume, tumor weight and survival rate were improved with the treatment of TPG. The decreased Ki67 positive cells of the TPG group indicated higher proliferation inhibition than the gefitinib group. The tumor mass displayed significant NIR fluorescence *in vivo* and *ex vivo*. Moreover, the fluorescence was sustained for over 24

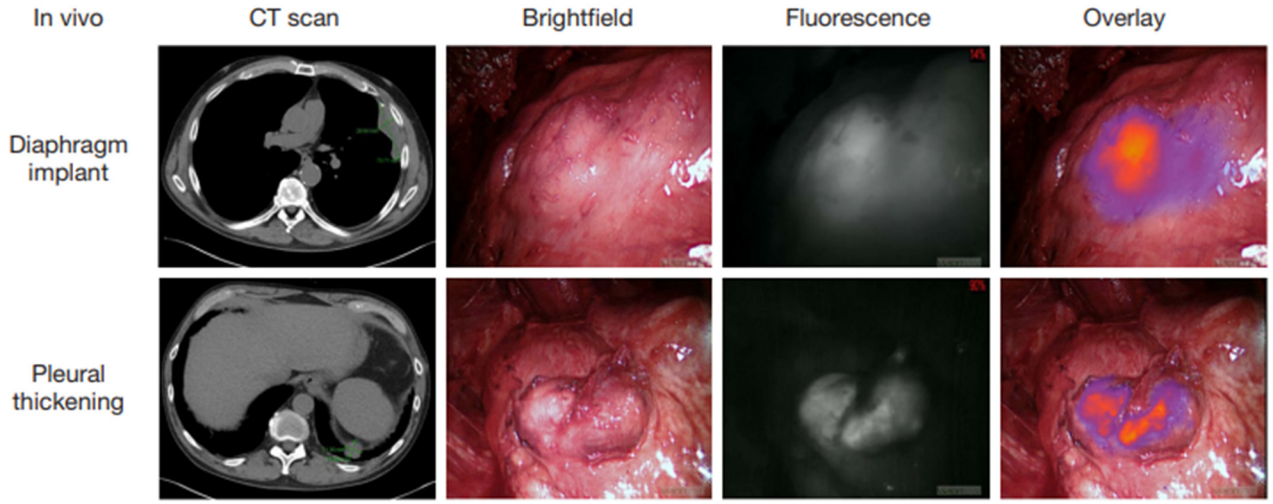

Fig. 14 Intraoperative near-infrared images for two mesothelioma representative patients. Preoperative CT scan, thoracoscopic view *in vivo*, fluorescence images, and merge of fluorescence images and brightfield images are shown from left to right. Reproduced with permission from ref. 128, Copyright 2017 *Translational Lung Cancer Research*.

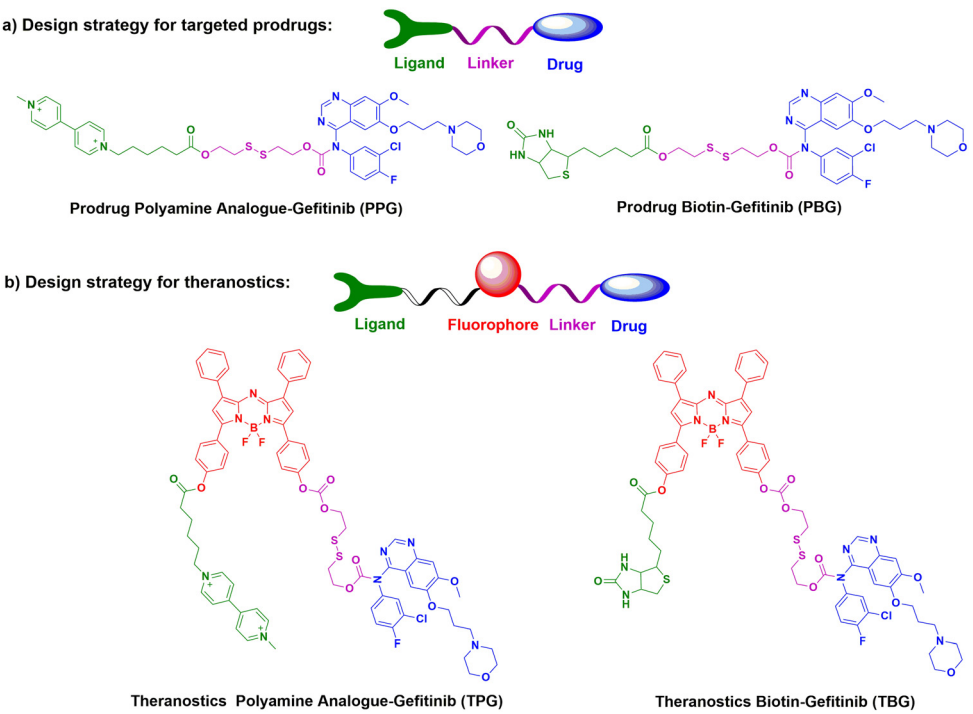

Fig. 15 The design strategies and chemical structures of part a) potential prodrugs PPG & PBG, and part b) theranostics TPG & TBG.

h, indicating the long-term gefitinib release. They also assessed the clinical applications of TPG in clinical diagnosis through flow cytometry. The preliminary diagnosis of NSCLC by TPG was proved to be reliable and rapid.

Yu's group also designed biotin theranostic TBG for NSCLC, with the combination of gefitinib and azo-BODIPY.[130] Biotin enhanced the TBG targeting ability for lung carcinoma. With the stronger inhibition of the EGFR related signal, TBG inhibited the growth of PC9 cells with lower IC50, compared with single gefitinib. TBG also showed a better anti-carcinoma effect than gefitinib *in vivo*. TBG showed better selectivity for the tumor mass with the help of NIR fluorescence than any other healthy organs. The drug release was sustained over 24 h.

Conclusions and perspective

Fluorescence bioimaging technology has become a promising chemical tool for biologists and physicians to investigate biological events because they can supply visual information

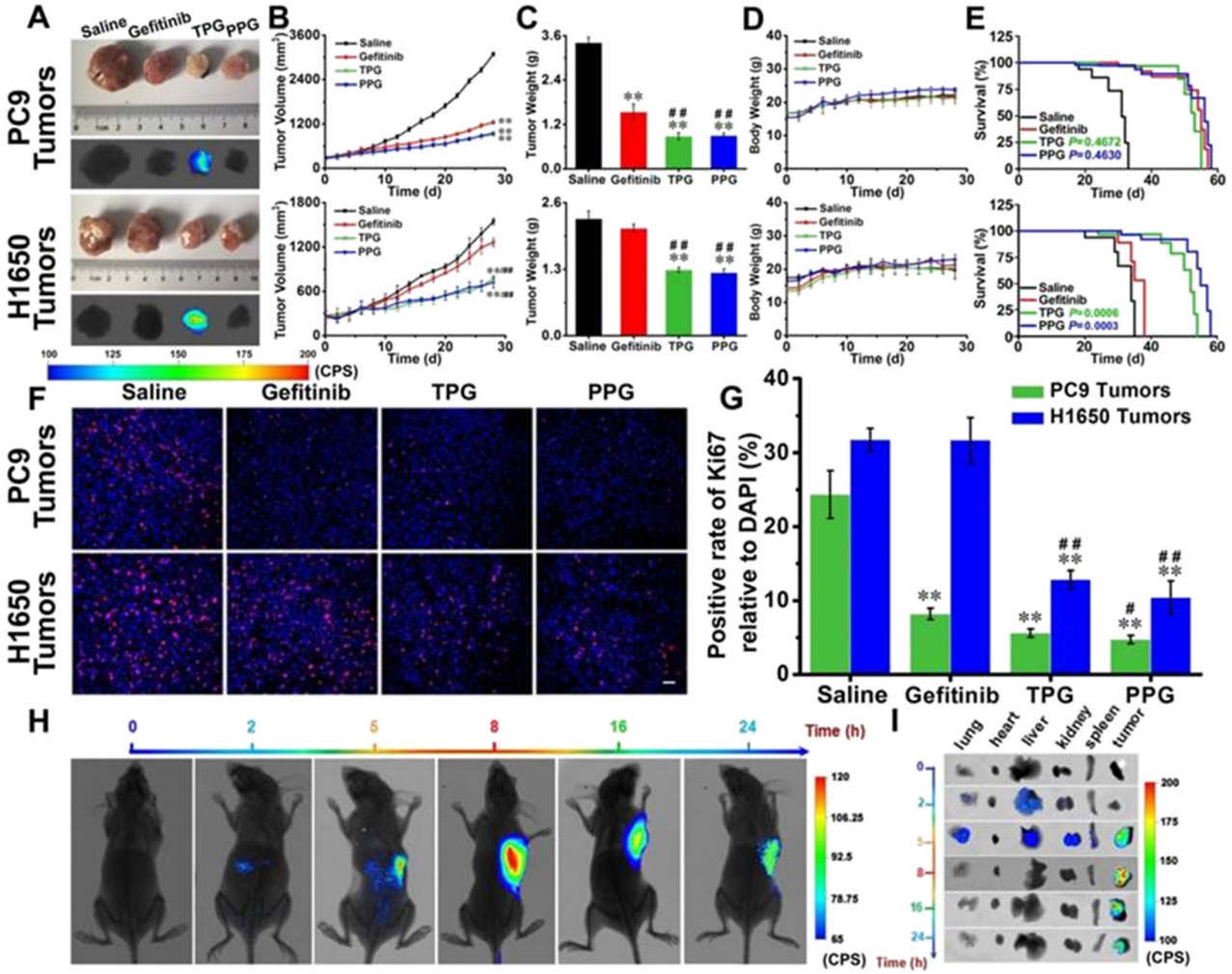

Fig. 16 Efficacy of fluorescence navigation in living mice. Thymus deficient mice bearing PC9 cells and H1650 cells were incubated with saline, gefitinib, TPG, and PPG, respectively. (A) The dissected solid tumors and their fluorescence images. (B) Tumor mass sizes. (C) Tumor mass weights. (D) Mouse body weights. (E) Survival curves. (F) Immunofluorescence staining of Ki67. (G) Statistical analysis derived from (F). (H) Fluorescence images of the mice at different time points after tail vein injection of TPG. (I) Fluorescence images of the dissected organs lung, heart, liver, kidney, spleen, and tumor masses from (G). Reproduced with permission from ref. 129, Copyright Ivyspring International Publisher.

with high spatial and temporal resolution *in situ* and in real time. Intraoperative molecular fluorescence imaging provides accurate tumor removal and the ability to determine whether tissue margins are still present while providing objective, real-time tumor visualization during surgical procedures. Compared with traditional probes with UV-visible emission wavelengths, near-infrared fluorescent probes have unique advantages, such as near-infrared emission which can prevent the interference of native biomolecular autofluorescence and achieve higher signal-to-noise ratios. The longer wavelengths of near-infrared fluorescent probes are able to acquire images in deeper tissue. Moreover, the near-infrared excitation and emission exhibit less damage to biological samples than UV-visible wavelengths of light. Over the past decade or so, near-infrared fluorescent probes have been developed to detect various biological species, monitor drug delivery, and perform surgical navigation *in vivo* and *in vitro*, but current tumor-targeted fluorescent probe libraries cannot identify all carcinomas, thus requiring the design of new tumor-specific fluorescent dyes used for carcinomas that are currently undetectable.

The early diagnosis and precise treatment of lung cancer are crucial for reducing patient mortality and improving the patient survival rate. Fluorescent probes for lung cancer are of importance in the clinical diagnosis and treatment. For diagnosis, the fluorescent probe will brighten the lung cancer tissue, allowing the operator to locate cancerous tissue surrounding healthy tissue with fluorescence guided endoscopy or percutaneous lung biopsy. The failure rate of biopsy and bleeding complications thereby decrease. For treatment, fluorescence tracing can aid to identify the risk of the tumor edge and distant metastasis for guiding accurate tumor resection, reducing the risk of tumor recurrence and metastasis, and preserving the patient's healthy lung tissue. Therefore, probes with good biocompatibility, high fluorescence intensity, and accurate targeting will benefit more clinical patients.

Fluorescence-guided surgery (FGS) is specifically targeted to and accumulates in tumors for molecular imaging, a technology capable of improving carcinoma patient outcomes by offering smart and non-invasive diagnosis, reducing total surgical time, and enabling more complete tumor resection. We believe that the ability to utilize new types of near-infrared fluorescent probes for intraoperative optical navigation can provide more sensitive and accurate strategies for carcinoma resection guidance, resulting in better surgical prognosis. However, in the process of research, it is also found that some fluorescent probes are only passively accumulated and cannot be used to distinguish tumors with inflammation. In the future, more precise targeting reagents need to be developed to solve this problem.

Conflicts of interest

The authors declared no conflict of interest.

Acknowledgements

This work was supported by the National Natural Science Foundation of China (No. 21904030, 22264013, 82202222 and 22204037), the Guangzhou Fundamentals and Applied Fundamentals Project (Grant 2023A04J0573), the Hainan Province Science and Technology Special Fund (Grants ZDYF2022SHFZ288), the Project supported by the Education Department of Hainan Province (Hnky2023ZD-12), the Hainan Province Clinical Medical Center (2021), the Natural Science Research Talent Project of Hainan Medical University (Grant JBGS202101), and the Project for Functional Materials and Molecular Imaging Science Innovation Group of Hainan Medical University.

References

1 Z. Guo, S. Park, J. Yoon and I. Shin, *Chem. Soc. Rev.*, 2014, **43**, 16–29.
2 M. Asgher, S. A. Qamar, M. Sadaf and H. M. N. Iqbal, *Biomed. Phys. Eng. Express*, 2020, **6**, 012003.
3 F. Yang, Q. Zhang, S. Huang and D. Ma, *J. Mater. Chem. B*, 2020, **8**, 7856–7879.
4 J. Rao, A. Dragulescu-Andrasi and H. Yao, *Curr. Opin. Biotechnol.*, 2007, **18**, 17–25.
5 W. Chyan and R. T. Raines, *ACS Chem. Biol.*, 2018, **13**, 1810–1823.
6 X. Wu, R. Wang, N. Kwon, H. Ma and J. Yoon, *Chem. Soc. Rev.*, 2022, **51**, 450–463.
7 J. I. Scott, Q. Deng and M. Vendrell, *ACS Chem. Biol.*, 2021, **16**, 1304–1317.
8 S. Luo, E. Zhang, Y. Su, T. Cheng and C. Shi, *Biomaterials*, 2011, **32**, 7127–7138.
9 Y. Mao, D. Yang, J. He and M. J. Krasna, *Hematol./Oncol. Clin. North Am.*, 2016, **25**, 439–445.
10 J. Jiao, J. Zhang, F. Yang, W. Song, D. Han, W. Wen and W. Qin, *Eur. J. Pharm. Biopharm.*, 2020, **152**, 123–143.
11 K. R. Tringale, J. Pang and Q. T. Nguyen, *Wiley Interdiscip. Rev.: Syst. Biol. Med.*, 2018, **10**, e1412.
12 S. Katsumata, K. Aokage, G. Ishii, S. Nakasone, T. Sakai, S. Okada, T. Miyoshi, K. Tane and M. Tsuboi, *J. Thorac. Oncol.*, 2019, **14**, 1408–1418.
13 H. Brody, *Nature*, 2020, **587**, S7.
14 K. Ganorkar, A. Samanta, S. Mukherjee, R. Joshi, S. Gupta, A. Sarkar and S. Ghosh, *J. Phys. Chem. B*, 2023, **127**, 104–120.
15 J. Chen, J. Xu, J. Xiang, T. Wan, H. Deng and D. Li, *Talanta*, 2023, **253**, 124056.
16 Q. Zhang, Y. Han, C. Li, X. Zou, F. Ma and C. Zhang, *Chem. Commun.*, 2022, **58**, 5538–5541.
17 L. Ao, T. Liao, L. Huang, S. Lin, K. Xu, J. Ma, S. Qiu, X. Wang and Q. Zhang, *Chem. Eng. J.*, 2022, **436**, 135204.
18 C. Li, H. Chen, X. Luo, J. Hu and C. Zhang, *Chem. Sci.*, 2021, **12**, 12407–12418.
19 Y. Zheng, J. Chen, Y. Li, Y. Xu, L. Chen, W. Chen, A. Liu, X. Lin and S. Weng, *Anal. Bioanal. Chem.*, 2021, **413**, 1605–1614.
20 F. Yang, D. Lin, L. Pan, J. Zhu, J. Shen, L. Yang and C. Jiang, *Anal. Chem.*, 2021, **93**(43), 14506–14513.
21 R. Liu, Y. Xu, K. Xu and Z. Dai, *Aggregate*, 2021, **2**, e23.
22 X. Zhang, T. Ren, F. Yang and L. Yuan, *Chin. Chem. Lett.*, 2021, **32**, 3890–3894.
23 S. Xu, W. Pan, T. Ren, S. Huan, L. Yuan and X. Zhang, *Chin. J. Chem.*, 2022, **40**, 1073–1082.
24 H. L. Stewart and D. J. S. Birch, *Methods Appl. Fluoresc.*, 2021, **9**, 4.
25 C. Qiu, Z. Cheng, C. Lv, R. Wang and F. Yu, *Chin. Chem. Lett.*, 2021, **32**, 2369–2379.
26 D. Xu, L. Li, C. Chu, X. Zhang and G. Liu, *Wiley Interdiscip. Rev.: Nanomed. Nanobiotechnol.*, 2020, **12**, e1635.
27 D. C. Hinshaw and L. A. Shevde, *Cancer Res.*, 2019, **79**, 4557–4566.
28 S. C. Casey, A. Amedei, K. Aquilano, A. S. Azmi, F. Benencia, D. Bhakta, A. E. Bilsland, C. S. Boosani, S. Chen, M. R. Ciriolo, S. Crawford, H. Fujii, A. G. Georgakilas, G. Guha, D. Halicka, W. G. Helferich, P. Heneberg, K. Honoki, W. N. Keith, S. P. Kerkar, S. I. Mohammed, E. Niccolai, S. Nowsheen, H. P. Vasantha Rupasinghe, A. Samadi, N. Singh, W. H. Talib, V. Venkateswaran, R. L. Whelan, X. Yang and D. W. Felsher, *Semin. Cancer Biol.*, 2015, **35**, S199–S223.
29 H. Wang, M. M. H. Yung, H. Y. S. Ngan, K. K. L. Chan and D. W. Chan, *Int. J. Mol. Sci.*, 2021, **22**, 6560.
30 B. Arneth, *Medicina*, 2019, **56**, 15.
31 E. E. Graves, M. Vilalta, I. K. Cecic, J. T. Erler, P. T. Tran, D. Felsher, L. Sayles, A. Sweet-Cordero, Q. T. Le and A. J. Giaccia, *Clin. Cancer Res.*, 2010, **16**, 4843–4852.
32 M. Höckel and P. Vaupel, *J. Natl. Cancer Inst.*, 2001, **93**, 266–276.
33 Y. C. Chae, V. Vaira, M. C. Caino, H. Y. Tang, J. H. Seo, A. V. Kossenkov, L. Ottobrini, C. Martelli, G. Lucignani, I. Bertolini, M. Locatelli, K. G. Bryant, J. C. Ghosh, S. Lisanti, B. Ku, S. Bosari, L. R. Languino, D. W. Speicher and D. C. Altieri, *Cancer Cell*, 2016, **30**, 257–272.

34 F. Xue, J. Chen and H. Chen, *Sci. China: Life Sci.*, 2020, **63**, 1786–1797.
35 D. Zhu, L. Xue, G. Li and H. Jiang, *Sens. Actuators, B*, 2016, **222**, 419–424.
36 X. Zhang, X. Li, W. Shi and H. Ma, *Chem. Commun.*, 2021, **57**, 8174–8177.
37 Y. Li, Y. Sun, J. Li, Q. Su, W. Yuan, Y. Dai, C. Han, Q. Wang, W. Feng and F. Li, *J. Am. Chem. Soc.*, 2015, **137**, 6407–6416.
38 T. Acker, J. Fandrey and H. Acker, *Cardiovasc. Res.*, 2006, **71**, 195–207.
39 K. Y. A. Lee, J. J. Kim, J. Lee, J. H. J. Lee, S. Sahu, H. Y. Kwon, S. J. Park, S. Y. Jang, J. S. Lee, Z. Wang, W. L. Tam, B. Lim, N. Y. Kang and Y. T. Chang, *Angew. Chem., Int. Ed.*, 2018, **57**, 2851–2854.
40 J. K. Kepa and D. Ross, *Biochem. Biophys. Res. Commun.*, 2003, **311**, 446–453.
41 S. R. Punganuru, H. R. Madala, V. Arutla, R. Zhang and K. S. Srivenugopal, *Sci. Rep.*, 2019, **9**, 8577.
42 W. Zhang, Y. Zhou, D. Li and T. Ma, *Spectrochim. Acta, Part A*, 2021, **252**, 119533.
43 J. J. Kim, Y. A. Lee, D. Su, J. Lee, S. J. Park, B. Kim, J. H. Jane Lee, X. Liu, S. S. Kim, M. A. Bae, J. S. Lee, S. C. Hong, L. Wang, A. Samanta, H. Y. Kwon, S. Y. Choi, J. Y. Kim, Y. H. Yu, H. H. Ha, Z. Wang, W. L. Tam, B. Lim, N. Y. Kang and Y. T. Chang, *J. Am. Chem. Soc.*, 2019, **141**, 14673–14686.
44 J. J. Schlager and G. Powis, *Int. J. Cancer*, 1990, **45**, 403–409.
45 S. Son, M. Won, O. Green, N. Hananya, A. Sharma, Y. Jeon, J. H. Kwak, J. L. Sessler, D. Shabat and J. S. Kim, *Angew. Chem., Int. Ed.*, 2019, **58**, 1739–1743.
46 E. M. Digby, O. Sadovski and A. A. Beharry, *Chemistry*, 2020, **26**, 2713–2718.
47 X. Zhang, K. Jiang, S. Jiang, F. Zhao, P. Chen, P. Huang and J. Lin, *Anal. Chem.*, 2022, **94**(40), 13770–13776.
48 T. Sato, S. Takahashi, T. Mizumoto, M. Harao, M. Akizuki, M. Takasugi, T. Fukutomi and J. Yamashita, *Surg. Oncol.*, 2006, **15**, 217–222.
49 S. Y. Liu, H. Xiong, R. R. Li, W. C. Yang and G. F. Yang, *Anal. Chem.*, 2019, **91**, 3877–3884.
50 X. Zhang, C. Jiang, T. He, F. Zhao, J. Qu, P. Huang and J. Lin, *Anal. Chem.*, 2022, **94**(7), 3227–3234.
51 W. E. Mitch and A. L. Goldberg, *N. Engl. J. Med.*, 1996, **335**, 1897–1905.
52 R. Weissleder, C. H. Tung, U. Mahmood and A. Bogdanov Jr., *Nat. Biotechnol.*, 1999, **17**, 375–378.
53 J. L. Figueiredo, H. Alencar, R. Weissleder and U. Mahmood, *Int. J. Cancer*, 2006, **118**, 2672–2677.
54 X. Chen, D. Lee, S. Yu, G. Kim, S. Lee, Y. Cho, H. Jeong, K. T. Nam and J. Yoon, *Biomaterials*, 2017, **122**, 130–140.
55 T. J. Mafireyi, M. Laws, J. W. Bassett, P. B. Cassidy, J. O. Escobedo and R. M. Strongin, *Angew. Chem., Int. Ed.*, 2020, **59**, 15147–15151.
56 Q. Hu, W. Zhu, J. Du, S. Long, W. Sun, J. Fan and X. Peng, *Chem. Commun.*, 2023, **59**, 294–297.
57 Y. Wang, T. Liu, E. Zhang, S. Luo, X. Tan and C. Shi, *Biomaterials*, 2014, **35**, 4116–4124.
58 Y. Hu, L. Shi, Y. Su, C. Zhang, X. Jin and X. Zhu, *Biomater. Sci.*, 2017, **5**, 792–799.
59 X. Zhang, N. He, Y. Huang, F. Yu, B. Li, C. Lv and L. Chen, *Sens. Actuators, B*, 2019, **282**, 69–77.
60 Y. Li, H. Wang, M. Wang, Y. Niu, J. Xing and N. Su, *Dyes Pigm.*, 2020, **181**, 108494.
61 M. Y. Lucero and J. Chan, *Nat. Chem.*, 2021, **13**, 1248–1256.
62 J. Dobson, G. F. de Queiroz and J. P. Golding, *Vet. J.*, 2018, **233**, 8–18.
63 J. Lyngbye, *Ugeskr. Laeg.*, 2007, **169**, 2873.
64 Z. Zhou, L. Zhang, Z. Zhang and Z. Liu, *Asian J. Pharm. Sci.*, 2021, **16**, 668–686.
65 A. El-Hussein, S. L. Manoto, S. Ombinda-Lemboumba, Z. A. Alrowaili and P. Mthunzi-Kufa, *Anti-Cancer Agents Med. Chem.*, 2021, **21**, 149–161.
66 T. G. Sutedja and P. E. Postmus, *J. Photochem. Photobiol., B*, 1996, **36**, 199–204.
67 J. Usuda, H. Kato, T. Okunaka, K. Furukawa, H. Tsutsui, K. Yamada, Y. Suga, H. Honda, Y. Nagatsuka, T. Ohira, M. Tsuboi and T. Hirano, *J. Thorac. Oncol.*, 2006, **1**, 489–493.
68 K. Furuse, M. Fukuoka, H. Kato, T. Horai, K. Kubota, N. Kodama, Y. Kusunoki, N. Takifuji, T. Okunaka and C. Konaka, *J. Clin. Oncol.*, 1993, **11**, 1852–1857.
69 H. Kato, K. Furukawa, M. Sato, T. Okunaka, Y. Kusunoki, M. Kawahara, M. Fukuoka, T. Miyazawa, T. Yana, K. Matsui, T. Shiraishi and H. Horinouchi, *Lung Cancer*, 2003, **42**, 103–111.
70 C. Lin, Y. Zhang, Q. Zhao, P. Sun, Z. Gao and S. Cui, Analysis of the short-term effect of photodynamic therapy on primary bronchial lung carcinoma, *Lasers Med. Sci.*, 2021, **36**(4), 753–761.
71 X. Yi, F. Wang, W. Qin, X. Yang and J. Yuan, *Int. J. Nanomed.*, 2014, **9**, 1347–1365.
72 X. Tan, S. Luo, D. Wang, Y. Su, T. Cheng and C. Shi, *Biomaterials*, 2012, **33**, 2230–2239.
73 V. Ramu, P. Kundu, P. Kondaiah and A. R. Chakravarty, *Inorg. Chem.*, 2021, **60**, 6410–6420.
74 H. Kobayashi and P. L. Choyke, *Acc. Chem. Res.*, 2019, **52**, 2332–2339.
75 Y. Maruoka, H. Wakiyama, P. L. Choyke and H. Kobayashi, *EBioMedicine*, 2021, **70**, 103501.
76 H. Kobayashi, A. Furusawa, A. Rosenberg and P. L. Choyke, *Int. Immunol.*, 2021, **33**, 7–15.
77 Y. Nakamura, Z. W. Ohler, D. Householder, T. Nagaya, K. Sato, S. Okuyama, F. Ogata, D. Daar, T. Hoa, P. L. Choyke and H. Kobayashi, *Mol. Cancer Ther.*, 2017, **16**(2), 408–414.
78 L. R. Saunders, A. J. Bankovich, W. C. Anderson, M. A. Aujay, S. Bheddah, K. Black, R. Desai, P. A. Escarpe, J. Hampl, A. Laysang, D. Liu, J. Lopez-Molina, M. Milton, A. Park, M. A. Pysz, H. Shao, B. Slingerland, M. Torgov, S. A. Williams, O. Foord, P. Howard, J. Jassem, A. Badzio, P. Czapiewski, D. H. Harpole, A. Dowlati, P. P. Massion, W. D. Travis, M. C. Pietanza, J. T. Poirier, C. M. Rudin, R. A. Stull and S. J. Dylla, *Sci. Transl. Med.*, 2015, **7**, 302ra136.
79 Y. Isobe, K. Sato, Y. Nishinaga, K. Takahashi, S. Taki, H. Yasui, M. Shimizu, R. Endo, C. Koike, N. Kuramoto, H. Yukawa, S. Nakamura, T. Fukui, K. Kawaguchi, T. F. Chen-

Yoshikawa, Y. Baba and Y. Hasegawa, *EBioMedicine*, 2020, **52**, 102632.
80 Y. Nishinaga, K. Sato, H. Yasui, S. Taki, K. Takahashi, M. Shimizu, R. Endo, C. Koike, N. Kuramoto, S. Nakamura, T. Fukui, H. Yukawa, Y. K. Baba, M. Kaneko, T. F. Chen-Yoshikawa, H. Kobayashi, Y. Kato and Y. Hasegawa, *Cells*, 2020, **9**, 1019.
81 K. Sato, T. Nagaya, P. L. Choyke and H. Kobayashi, *Theranostics*, 2015, **5**, 698–709.
82 A. Mochida, F. Ogata, T. Nagaya, P. L. Choyke and H. Kobayashi, *Bioorg. Med. Chem.*, 2018, **26**, 925–930.
83 M. T. Olson, Q. P. Ly and A. M. Mohs, *Mol. Imaging Biol.*, 2019, **21**, 200–218.
84 C. G. Patil, D. G. Walker, D. M. Miller, P. Butte, B. Morrison, D. S. Kittle, S. J. Hansen, K. L. Nufer, K. A. Byrnes-Blake, M. Yamada, L. L. Lin, K. Pham, J. Perry, J. Parrish-Novak, L. Ishak, T. Prow, K. Black and A. N. Mamelak, *Neurosurgery*, 2019, **85**, E641–E649.
85 C. R. Lanahan, B. N. Kelly, M. A. Gadd, M. C. Specht, C. L. Brown, K. S. Hughes, R. Tang, U. Rai, E. F. Brachtel, T. Rice-Stitt and B. L. Smith, *Breast Cancer Res. Treat.*, 2021, **187**, 145–153.
86 F. Azari, G. Kennedy, E. Bernstein, J. Delikatny, J. Y. K. Lee, J. Kucharczuk, P. S. Low and S. Singhal, *Mol. Imaging Biol.*, 2023, **25**, 85–96.
87 C. E. S. Hoogstins, L. S. F. Boogerd, B. G. Sibinga Mulder, J. S. D. Mieog, R. J. Swijnenburg, C. J. H. van de Velde, A. Farina Sarasqueta, B. A. Bonsing, B. Framery, A. Pèlegrin, M. Gutowski, F. Cailler, J. Burggraaf and A. L. Vahrmeijer, *Ann. Surg. Oncol.*, 2018, **25**, 3350–3357.
88 H. Hyun, M. Henary, T. Gao, L. Narayana, E. A. Owens, J. H. Lee, G. Park, H. Wada, Y. Ashitate, J. V. Frangioni and H. S. Choi, *Mol. Imaging Biol.*, 2016, **18**, 52–61.
89 H. Kobayashi, P. L. Choyke and M. Ogawa, *Curr. Opin. Chem. Biol.*, 2016, **33**, 32–38.
90 E. A. Azzopardi, S. E. Owens, M. Murison, D. Rees, M. Anne Sawhney and L. W. Francis, *J. Controlled Release*, 2017, **249**, 123–130.
91 D. A. Hudson, J. L. Caplan and C. Thorpe, *Biochemistry*, 2018, **57**, 1178–1189.
92 J. Liu, J. C. Fraire, S. C. De Smedt, R. Xiong and K. Braeckmans, *Small*, 2020, **16**, e2000146.
93 T. Nagaya, Y. A. Nakamura, P. L. Choyke and H. Kobayashi, *Front. Oncol.*, 2017, **7**, 314.
94 K. M. Schebesch, A. Brawanski, C. Hohenberger and J. Hohne, *Turk. Neurosurg.*, 2016, **26**, 185–194.
95 C. Cavallo, C. De Laurentis, I. G. Vetrano, J. Falco, M. Broggi, M. Schiariti, P. Ferroli and F. Acerbi, *J. Neurosurg. Sci.*, 2018, **62**, 690–703.
96 S. Ruia and K. Tripathy, Fluorescein Angiography, in *StatPearls*, StatPearls Publishing, Treasure Island (FL), 2022.
97 D. Qaiser, A. Sood, D. Mishra, O. P. Kharbanda, A. Srivastava, S. D. Gupta, R. M. Pandey, R. Yadav, K. Bhatt and R. Kumawat, *Photodiagn. Photodyn. Ther.*, 2020, **31**, 101824.
98 M. Bretonnier, X. Morandi and P. J. Le Reste, *J. Clin. Neurosci.*, 2019, **70**, 226–228.
99 S. Dinslage, M. Diestelhorst, A. Weichselbaum and R. Süverkrüp, *Br. J. Ophthalmol.*, 2002, **86**, 1114–1117.
100 M. B. Reinhart, C. R. Huntington, L. J. Blair, B. T. Heniford and V. A. Augenstein, *Surg. Innov.*, 2016, **23**, 166–175.
101 J. W. Verjans, E. A. Osborn, G. J. Ughi, M. A. Calfon Press, E. Hamidi, A. P. Antoniadis, M. I. Papafaklis, M. F. Conrad, P. Libby, P. H. Stone, R. P. Cambria, G. J. Tearney and F. A. Jaffer, *JACC Cardiovasc. Imaging*, 2016, **9**, 1087–1095.
102 C. Tian, X. Chen, J. Cao and L. Yang, *Oncol. Lett.*, 2018, **15**, 5760–5766.
103 J. Meira, M. L. Marques, F. Falcão-Reis, E. Rebelo Gomes and Â. Carneiro, *Clin. Ophthalmol.*, 2020, **14**, 171–178.
104 J. He, L. Yang, W. Yi, W. Fan, Y. Wen, X. Miao and L. Xiong, *Mol. Imaging*, 2017, **16**, 1536012117722911.
105 Q. Chen, L. Xu, C. Liang, C. Wang, R. Peng and Z. Liu, *Nat. Commun.*, 2016, **7**, 13193.
106 C. Egloff-Juras, L. Bezdetnaya, G. Dolivet and H. P. Lassalle, *Int. J. Nanomed.*, 2019, **14**, 7823–7838.
107 H. Chiu, K. Chao, H. Liu, T. Wen, H. Chen, Y. Wu, M. J. Hsieh, C. Wu and P. Liu, *J. Thorac. Dis.*, 2016, **8**, S744–S748.
108 S. Kaneko and S. Kaneko, *Int. J. Biomed. Imaging*, 2016, 6135293.
109 G. Guney Eskiler, A. Deveci Ozkan, E. Sozen Kucukkara, A. F. Kamanlı, B. Gunoğlu and M. Z. Yıldız, *Photodiagn. Photodyn. Ther.*, 2020, **31**, 101854.
110 M. H. Gold and M. P. Goldman, *Dermatol. Surg.*, 2004, **30**, 1077–1084.
111 Y. Jiang, Y. Liu, S. Fang and M. Ji, *J. Nanosci. Nanotechnol.*, 2020, **20**, 1–14.
112 H. D. Aoun, P. J. Littrup, K. E. Heath, B. Adam, M. Prus, R. Beydoun and F. Baciewcz, *J. Vasc. Interv. Radiol.*, 2020, **31**, 1682.
113 A. Gregor, H. Ujiie and K. Yasufuku, *Gen. Thorac. Cardiovasc. Surg.*, 2020, **68**, 1061–1078.
114 K. J. Hachey and Y. L. Colson, *Semin. Thorac. Cardiovasc. Surg.*, 2014, **26**, 201–209.
115 D. M. Gilmore, O. V. Khullar and Y. L. Colson, *J. Thorac. Cardiovasc. Surg.*, 2012, **144**, S80–S84.
116 D. M. Gilmore, O. V. Khullar, M. T. Jaklitsch, L. R. Chirieac, J. V. Frangioni and Y. L. Colson, *J. Thorac. Cardiovasc. Surg.*, 2013, **146**, 562–570.
117 K. J. Hachey, C. S. Digesu, K. W. Armstrong, D. M. Gilmore, O. V. Khullar, B. Whang, H. Tsukada and Y. L. Colson, *J. Thorac. Cardiovasc. Surg.*, 2017, **154**, 1110–1118.
118 C. S. Digesu, K. J. Hachey, D. M. Gilmore, O. V. Khullar, H. Tsukada, B. Whang, L. R. Chirieac, R. F. Padera, M. T. Jaklitsch and Y. L. Colson, *J. Thorac. Cardiovasc. Surg.*, 2018, **155**, 1280–1291.
119 S. Zhao, X. Guo, M. Taniguchi, K. Kondo, S. Yamada, C. Gu and H. Uramoto, *Anticancer Res.*, 2020, **40**, 1875–1882.
120 H. Li, J. Zhou, C. Chi, Y. Mao, F. Yang, J. Tian and J. Wang, *J. Thorac. Dis.*, 2016, **8**(7), 1841–1845.
121 R. Zhang, A. B. Schroeder, J. J. Grudzinski, E. L. Rosenthal, J. M. Warram, A. N. Pinchuk, K. W. Eliceiri,

J. S. Kuo and J. P. Weichert, *Nat. Rev. Clin. Oncol.*, 2017, **14**, 347–364.

122 J. D. Predina, A. Newton, C. Connolly and S. Singhal, *J. Cardiothorac. Surg.*, 2017, **12**, 110.

123 J. J. Keating, J. J. Runge, S. Singhal, S. Nims, O. Venegas, A. C. Durham, G. Swain, S. Nie, P. S. Low and D. E. Holt, *Cancer*, 2017, **123**(6), 1051–1060.

124 L. Zhong, W. Hu, S. Li, Z. Wei, Z. Zhu, G. Jin, H. Zhang, Y. Pang and J. Yu, *Videosurgery and Other Miniinvasive Techniques*, 2019, **14**, 545–550.

125 Y. Mao, C. Chi, F. Yang, J. Zhou, K. He, H. Li, X. Chen, J. Ye, J. Wang and J. Tian, *Eur. J. Cardiothorac. Surg.*, 2017, **52**, 1190–1196.

126 T. Wen, Y. Liu, Y. Fang, M. J. Hsieh and K. Chao, *Surg. Endosc.*, 2018, **32**, 4673–4680.

127 K. Kim, H. Quan, B. H. Choi, J. H. Park, K. N. Han, Y. Choi, B. M. Kim and Y. H. Choi, *Eur. J. Cardiothorac. Surg.*, 2016, **49**, 1497–1502.

128 G. T. Kennedy, A. Newton, J. Predina and S. Singhal, Intraoperative near-infrared imaging of mesothelioma, *Transl. Lung Cancer Res.*, 2017, **6**(3), 279–284.

129 X. Song, X. Han, F. Yu, X. Zhang, L. Chen and C. Lv, *Theranostics*, 2018, **8**(8), 2217–2228.

130 X. Song, R. Wang, J. Gao, X. Han, J. Jin, C. Lv and F. Yu, *Chin. Chem. Lett.*, 2022, **33**, 1567–1571.